NUREG/CR-4121
MEA-2053

The Effects of Sulfur Chemistry and Flow Rate on Fatigue Crack Growth Rates in LWR Environments

Prepared by W. H. Cullen/MEA
M. Kemppainen, H. Hanninen, K. Torronen/TRC

Materials Engineering Associates, Inc.

Technical Research Centre of Finland

Prepared for
U.S. Nuclear Regulatory
Commission

GPO Printed copy price: $4.00

NUREG/CR-4121
MEA-2053

The Effects of Sulfur Chemistry and Flow Rate on Fatigue Crack Growth Rates in LWR Environments

Manuscript Completed: January 1985
Date Published: February 1985

W. H. Cullen, Materials Engineering Associates, Inc.
M. Kemppainen, H. Hanninen, K. Torronen, Technical Research Centre of Finland

Materials Engineering Associates, Inc.
9700-B George Palmer Highway
Lanham, MD 20706

Subcontractor:
Technical Research Centre of Finland
Vuorimiehentie 5
SF-02150 Espoo 15
Finland

Prepared for
Division of Engineering Technology
Office of Nuclear Regulatory Research
U.S. Nuclear Regulatory Commission
Washington, D.C. 20555
NRC FIN B8900

ABSTRACT

Fatigue crack growth rate tests, at a load ratio of 0.2, have been conducted on steels of low, medium and high sulfur contents (0.004%, 0.013% and 0.025%) in PWR water at both low and high flow rates. Crack growth rates show no dependence on flow rate, but are strongly dependent on sulfur content, with a large proportion of environmental assistance for the highest sulfur contents. Tests of low and high sulfur content steels at a load ratio of 0.7 show relatively little environmental assistance in either case. The fractography of these specimens shows the usual brittle appearance for environmentally-assisted fatigue crack growth. In addition, the opposing fracture surfaces match perfectly, indicating that little or no dissolution of the metal matrix has occurred, and there is very little plastic flow associated with the fatigue cracking process. The X-ray photoelectron emission examination of the fracture surface oxides shows that FeS and FeS_2 coexist in the oxide layer, suggesting that the conditions within the crack enclave involved near-neutral pH and cathodic potentials.

CONTENTS

LIST OF FIGURES

LIST OF FIGURES

ACKNOWLEDGEMENT

The authors would like to acknowledge the efforts of Robert E. Taylor, MEA, for assistance in conducting this research effort. The XPS examination of the oxide was carried out by Dr. Martti Vulli, Dept. of Physics, Technical University of Tampere, Finland. Appreciation is also extended to Dr. Frank J. Loss, MEA, who provided program management during the course of this research. The continuing support of the NRC program manager, M. Vagins, is appreciated greatly.

1. INTRODUCTION

Several variables influence fatigue crack growth rates of piping and pressure vessel steels in light water reactor (LWR) environments. Since the first research results became available in 1971 and the present time, the identity and degree of influence of several of these variables have been well quantified. On the other hand, several variables have resisted accurate and convincing enumeration owing to inconsistent results from different laboratories performing nominally the same test, often with specimens from the same heat of steel. The research described in this report was carried out in an attempt to accurately define the role of sulfur chemistry and water flow rate on the fatigue crack growth rates in PWR environments. The tests were conducted using multiple-specimen "daisy chains" of steels with differing sulfur contents, to allow the direct comparison of crack growth rates under conditions which were common to all the specimens. The crack growth rate results are supported by fractographic investigations, and examinations of the fatigue fracture surface oxides using X-ray photoelectron spectroscopic (XPS) techniques.

2. REVIEW OF PUBLISHED RESULTS

The suggestion that sulfur content could have an effect on the fatigue crack growth rates of pressure vessel steels in pressurized water reactor (PWR) environments began to enter the literature about 1981 (Ref. 1). As the idea began to develop in more depth, the International Cyclic Crack Growth Rate group endorsed research to address this topic in particular, as a way to sort out some of the apparent discrepancies in results between various laboratories. Several research efforts sprang out of this interest. Examples of these results and conclusions are described below. A composite table giving the chemical compositions of the steels tested at the various laboratories is given in Table 1, and the sulfur contents are given in the legends of the appropriate graphs. The orientation designations are given using the ASTM nomenclature (Ref. 2), which is illustrated in Fig. 1.

The most comprehensive series of tests has been conducted by Bamford (Refs. 3 to 5), who has completed a matrix of tests of steels with various sulfur contents, using specimens of different orientations, tested at load ratios (R) of 0.2 and 0.7, and a 17-mHz sinusoidal waveform. Examples of these results are shown in Figs. 2 through 4. These data sets, for a low sulfur steel, show an increase in growth rates with an increase in load ratio, and little, if any, dependence on specimen orientation. Figure 4, for a steel of higher sulfur content, should be compared with Fig. 2, for the same load ratio. This comparison shows a significant increase in growth rates, along with a partitioning of the data for the different specimen orientations at the higher ΔK levels.

Parallel results have been obtained by Slama and coworkers (Ref. 1). Figure 5 shows results for steels of two sulfur levels, tested under PWR conditions at a load ratio of 0.2 and a 17-mHz triangular

Table 1 Chemical Compositions of Steels Described in This Report

Reference	Identification	C	Mn	P	S	Si	Mo	Ni	Cr	Cu	Al	Co	Sn	V
6	63758.1	0.185	1.395	0.01	0.006	0.195	0.485	0.655	0.130	0.095	0.002	-----	-----	-----
6	C8938	0.21	1.24	0.016	0.012	0.2	0.49	0.66	0.08	0.09	-----	0.013	0.012	-----
3	TW	0.21	1.38	0.008	0.004	0.21	0.56	0.67	-----	0.08	-----	-----	-----	-----
4	PN	0.21	1.33	0.012	0.016	0.22	0.53	0.56	-----	0.13	-----	-----	-----	-----
This report	1HT	0.19	1.280	0.009	0.013	0.250	0.550	0.610	0.040	0.100	-----	-----	-----	0.004
Ref. 4 and this report	CQ2	0.21	1.28	0.006	0.025	0.24	0.53	0.56	-----	0.12	-----	-----	-----	-----
This report	W7	0.23	1.40	0.005	0.004	0.25	0.57	0.70	-----	-----	-----	-----	-----	-----
7	0.025%S	0.23	1.33	0.011	0.025	0.23	0.48	0.66	-----	-----	-----	-----	-----	-----
7	0.006%S	0.185	1.395	0.01	0.006	0.195	0.485	0.655	0.130	0.095	0.002	-----	-----	-----

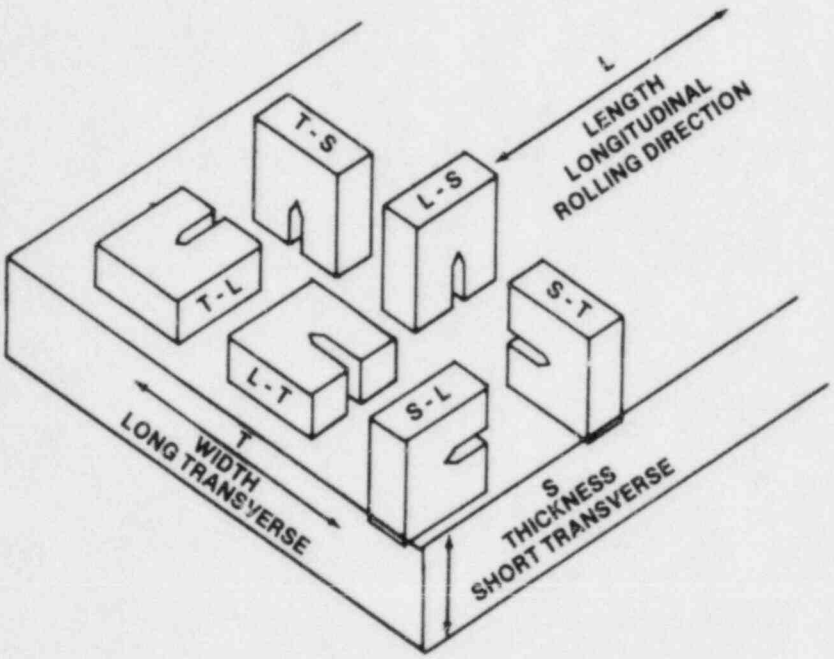

Fig. 1 A schematic showing the orientation nomenclature used in this report. This is the standard nomenclature from ASTM E 399.

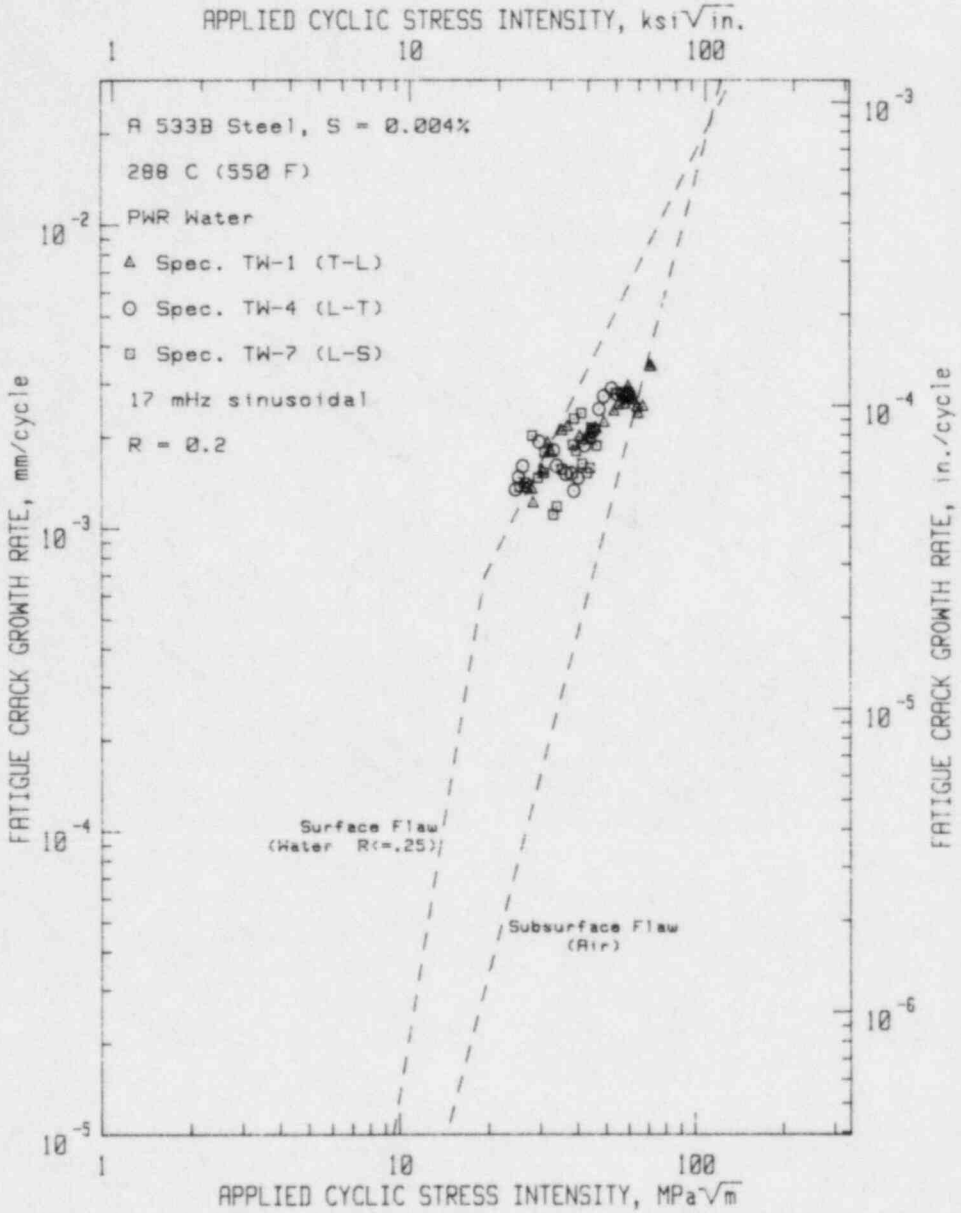

Fig. 2 Fatigue crack growth rates vs. applied cyclic ΔK for a steel of low sulfur content tested at a load ratio of 0.2. Although low in sulfur, this steel exhibits rather high growth rates. Reference lines taken from ASME Boiler and Pressure Vessel Code (Ref. 8). Data from Ref. 3.

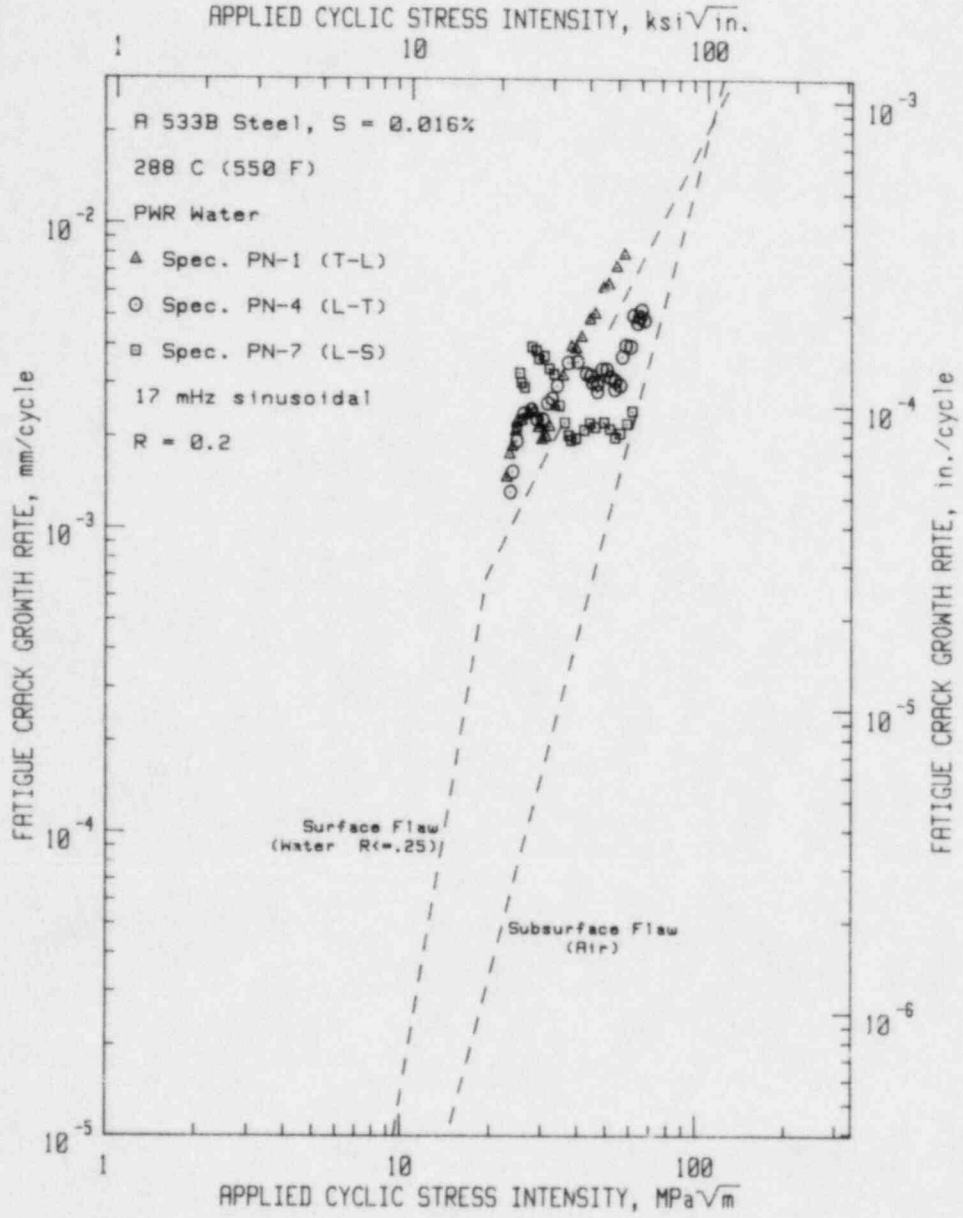

Fig. 3 Fatigue crack growth rates vs. applied cyclic ΔK for a steel of medium sulfur content tested at a load ratio of 0.2. These results, compared with Fig. 2, show an increase in growth rates. Data from Ref. 4.

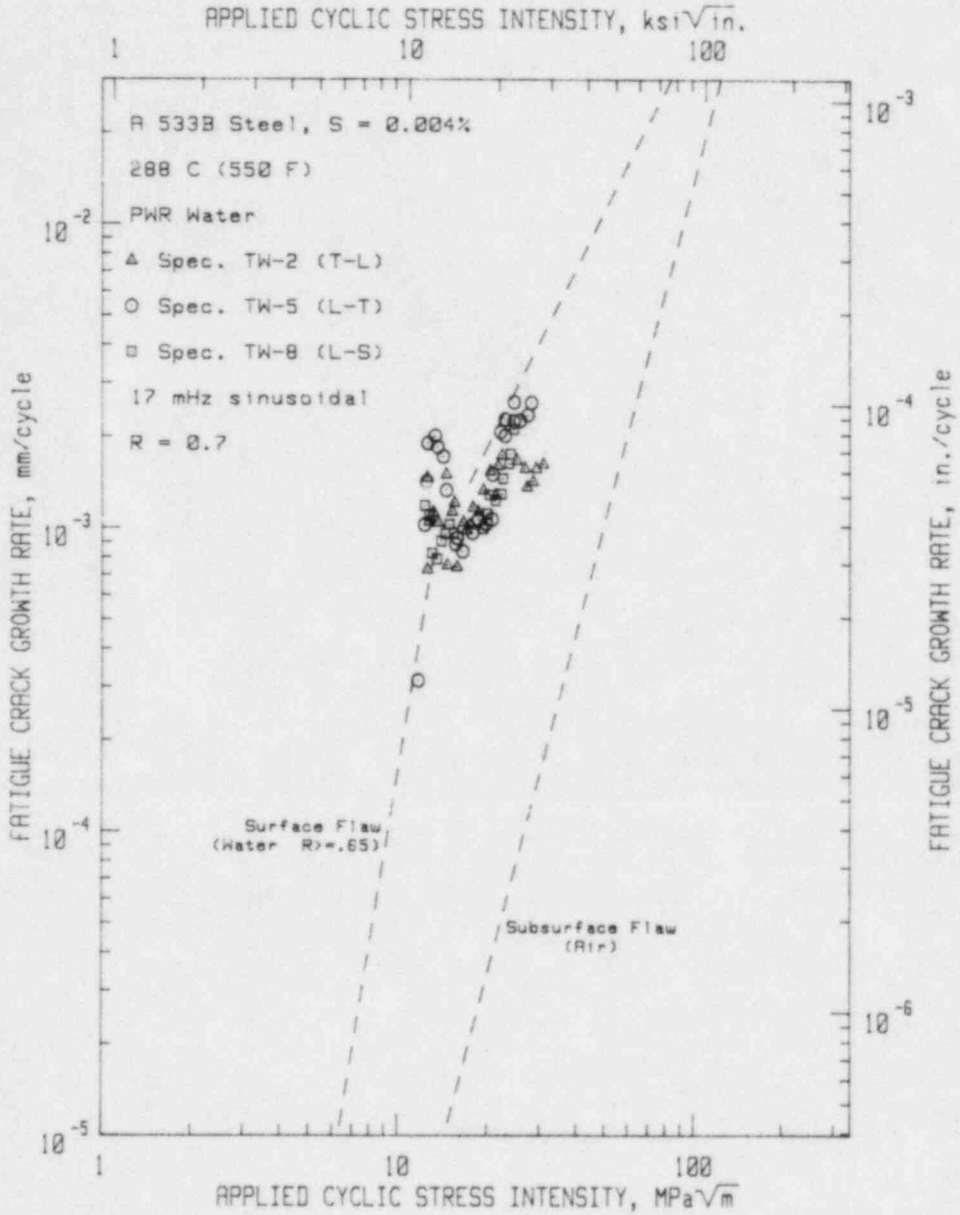

Fig. 4 Fatigue crack growth rates vs. applied cyclic ΔK for a steel of low sulfur content tested at a load ratio of 0.7. Data from Ref. 3.

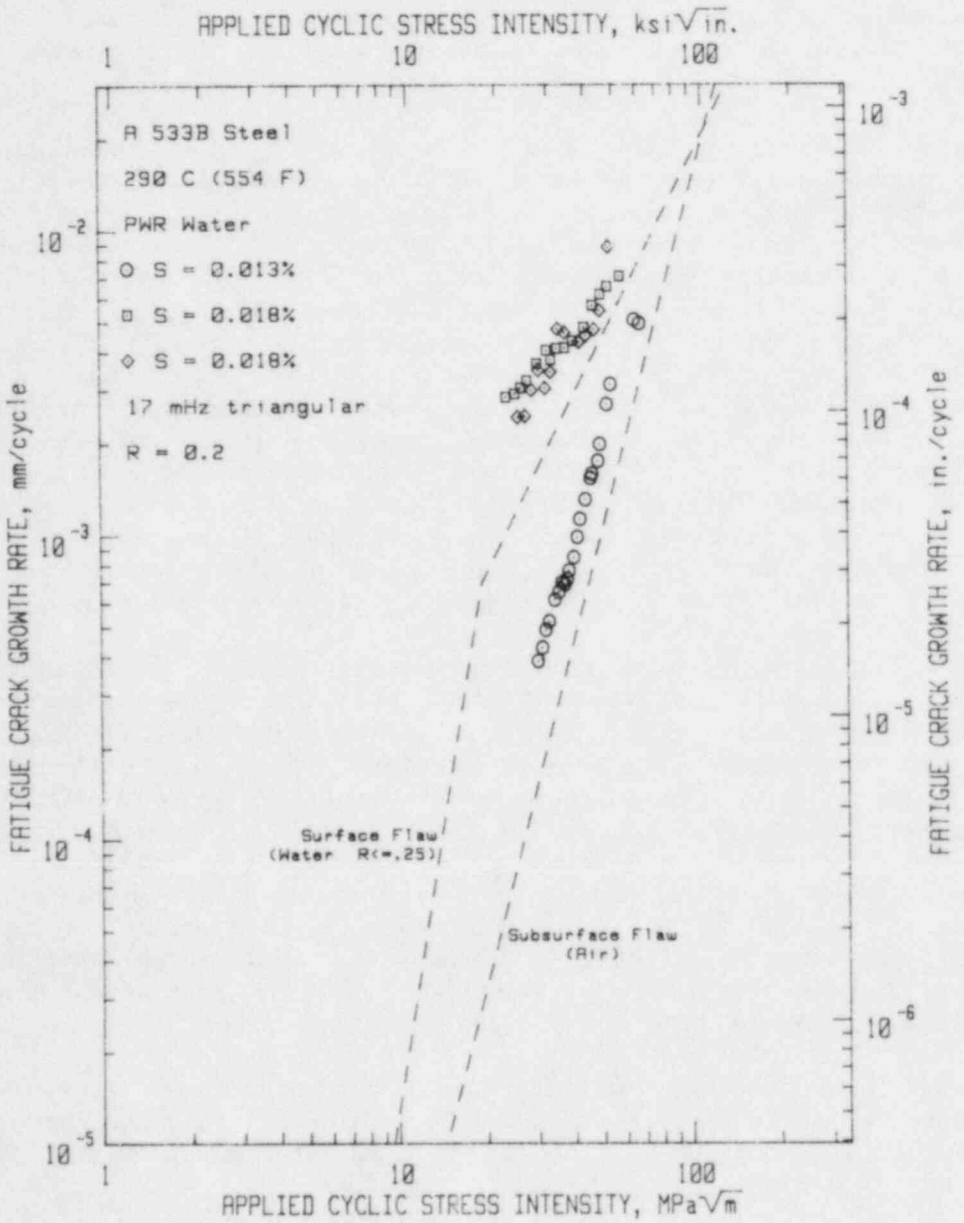

Fig. 5 Fatigue crack growth rates vs. applied cyclic ΔK for steels of two different sulfur contents, tested at a load ratio of 0.2 and a 17-mHz triangular waveform. Data from Ref. 1.

waveform. Concurrent research, also described in Reference 1, showed that triangular waveforms yielded consistently lower growth rates than sinusoidal waveforms, at least for steels of 0.009% and 0.013% sulfur contents. However, these data sets show that increasing the sulfur content to 0.018% results in growth rates which reside well outside the ASME reference line for $R \leq 0.25$, in spite of the triangular waveform.

Concurrent research at the UKAEA-Harwell laboratory produced crack growth rate results which were consistently lower than results at other laboratories, and Scott and Bamford engaged in a two-laboratory intercomparison study (Ref. 6) to try to sort out the reason for the discrepancy. Results of nominally identical tests of low (0.006%) and medium (0.012%) sulfur steels at both laboratories yielded the results shown in Fig. 6, with the UKAEA results (shaded symbols) a factor of ten or more lower than the Westinghouse results. Additional tests at Harwell, on steels of even higher sulfur contents, consistently yielded results well below the ASME reference lines for the appropriate load ratio (Ref. 9). However, Scott has published results of tests at considerably higher test frequencies and load ratios which show higher growth rates and a "plateau" or ΔK-independent range. Scott has developed a strain-rate model which accounts for the increase in growth rates with increasing load ratio and frequency.

Van Der Sluys (Ref. 7) has completed a unique test of a composite specimen, composed of sections of steel of different sulfur contents, electron beam welded together and formed into a specimen such that the crack proceeded through the various sections. The results of constant ΔK tests on this specimen are shown in Fig. 7. These results show clearly the influence of the sulfur content on crack growth rates, and the dependence on test frequency, for the higher sulfur content section, appears to show increasing growth rates with decreasing test frequency. Growth rates at 10 mHz, the closest comparison to the 17-mHz frequency cited above, straddle the ASME water environment reference line for the high sulfur steel, but are just above the air environment reference line for the lower sulfur content section.

Against this background, MEA undertook a series of two multispecimen tests, using steels of three different sulfur contents in each daisy chain, and conducted one test in a low-flow rate environment, and the other test in a high flow rate environment.

3. EXPERIMENTAL PROCEDURES

The MEA tests were carried out in a multispecimen autoclave capable of testing four 2T-CT [51-mm (2-in.) thick] specimens in a daisy chain. Each specimen was instrumented with an LVDT* in order to measure the crack mouth opening of the specimen. Crack mouth opening and load readings were used in an experimentally-determined formula to

* Linear Variable Differential Transformer

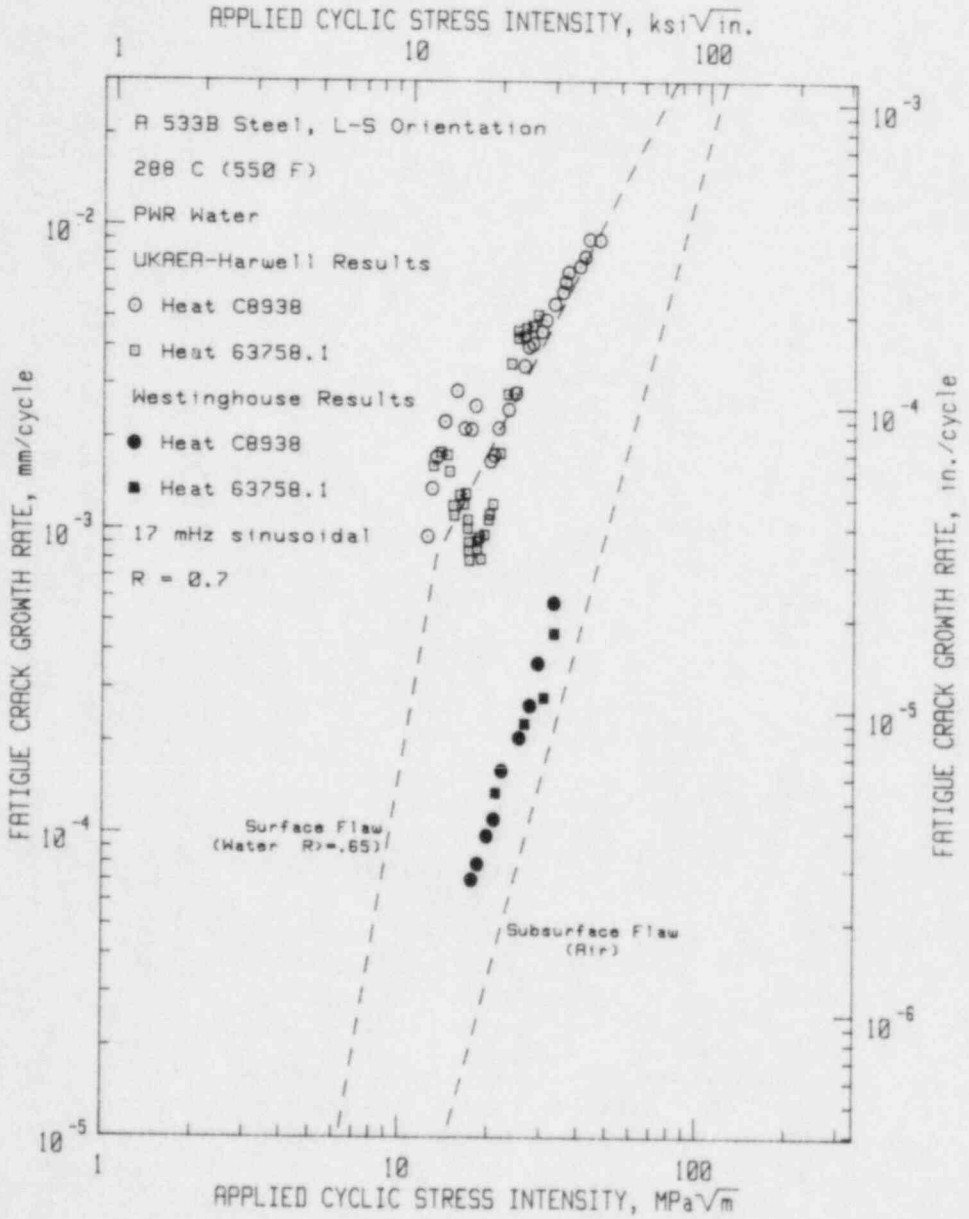

Fig. 6 Fatigue crack growth rates vs. applied cyclic ΔK for steels of low sulfur contents, tested under similar conditions at two different laboratories. Data from Ref. 6.

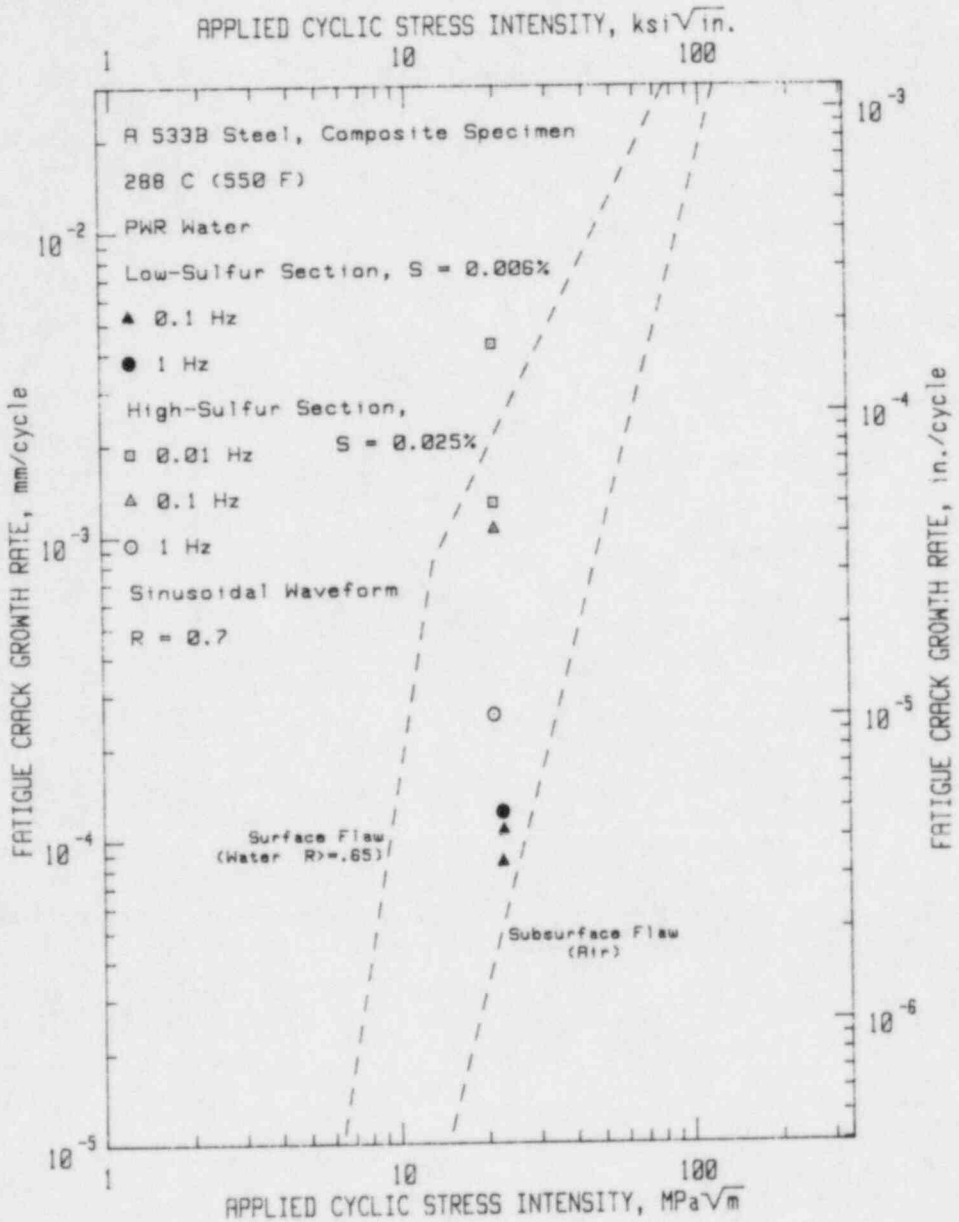

Fig. 7 Fatigue crack growth rates vs. applied cyclic ΔK for a composite specimen tested in constant ΔK mode. Low sulfur section results are shaded. Data from Ref. 7.

calculate the crack lengths in the specimen while the tests were underway. Data acquisition was carried out by a computer-based, data acquisition system which also monitored the cycle counts, system water chemistry, and other system parameters. The operation of these systems is described in earlier reports (Refs. 10 and 11).

The water pressurization and circulation system for these autoclaves is a recirculating system, with the system change rate being about two-to-three gallons per hour. Pressurized, high-temperature water pumps are used to obtain the circulation rates within the autoclave. The flow rates are established by throttle valves and measured by calibrated flow meters. The flow rates used in these tests were 50 liters per hour and 1000 liters per hour. The autoclave volume is about 140 liters. Water was directed towards the front faces of the specimens, and into the notch by a manifold system shown in Fig. 8.

The water used in this autoclave system had the nominal PWR chemistry which is specified in Table 2. Typical analyses of the water for these and other constituents are shown in Table 3. The chloride content is slightly above the specification, and is probably due to leakage from the dissolved oxygen sensor. The sulfate and phosphate contents are not covered in the specification, but are felt to be moderately high, but not to the point which would cause measureable change in the fatigue crack growth results. Since the time of these tests, an on-line water cleanup system has been installed on this autoclave circulation loop.

Specimens were prepared from plate pieces which were provided to MEA by Westinghouse (CQ2) and Electric Power Research Institute (1HT). The W7 plate and W8B weld were from MEA stock. The identification and chemical composition for these steels is given in Table 1. The microstructures of the steels are shown in Fig. 9. The CQ2 steel may have a small amount of tempered martensite mixed in with the predominately bainitic matrix. The other steels are bainitic. The orientation of all specimens was T-L, using the standard ASTM designations.

Table 2 Water Chemistry Specifications

Boron (as boric acid)	1000 ppm
Lithium (as lithium hydroxide)	1 ppm
Chloride ions	< 0.15 ppm
Fluoride ions	< 0.10 ppm
Dissolved oxygen	± 1 ppb
Dissolved hydrogen (saturation)	30 to 50 cm^3/kg water

All other metallic or ionic species should be at about trace levels. Some iron, both in solid and soluble form is the inevitable result of a corroding specimen.

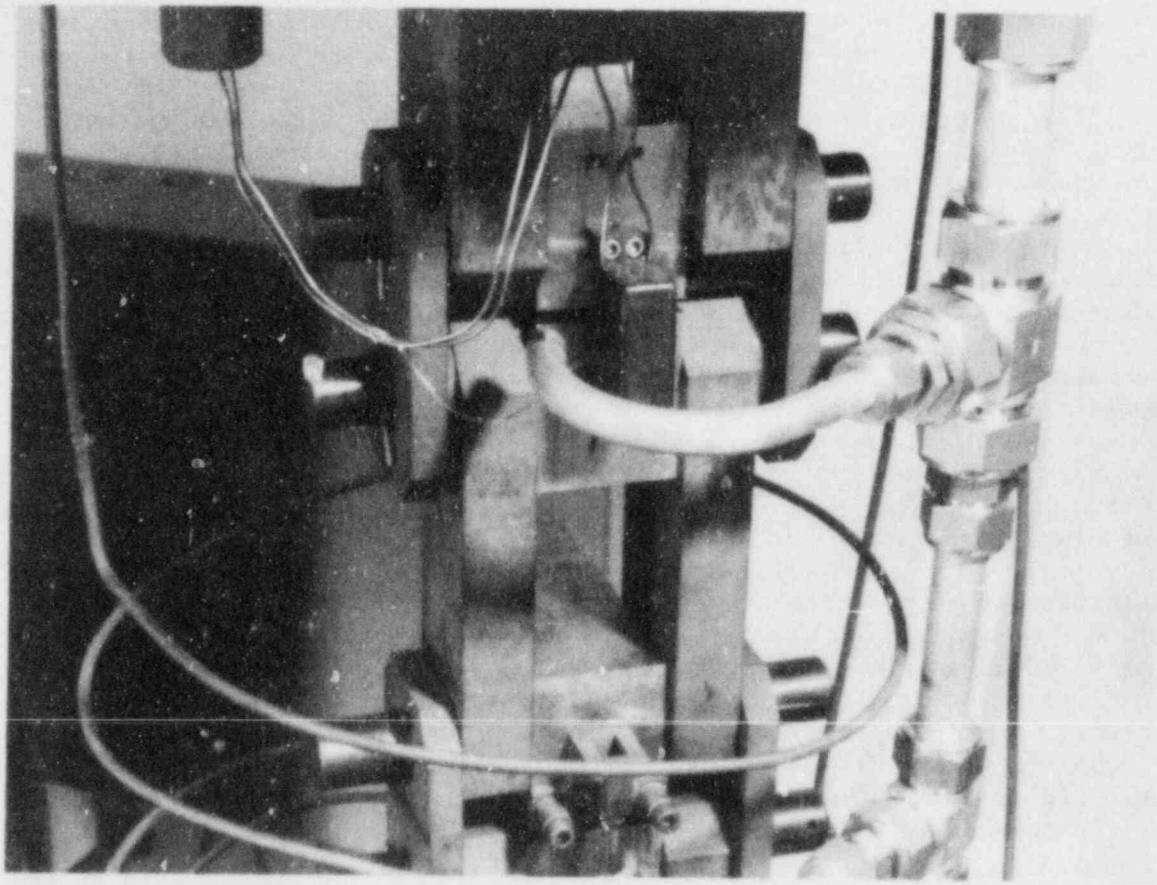

Fig. 8 Photograph of the daisy chain of specimens, showing part of the manifold system to direct the flow toward the mouth of each specimen.

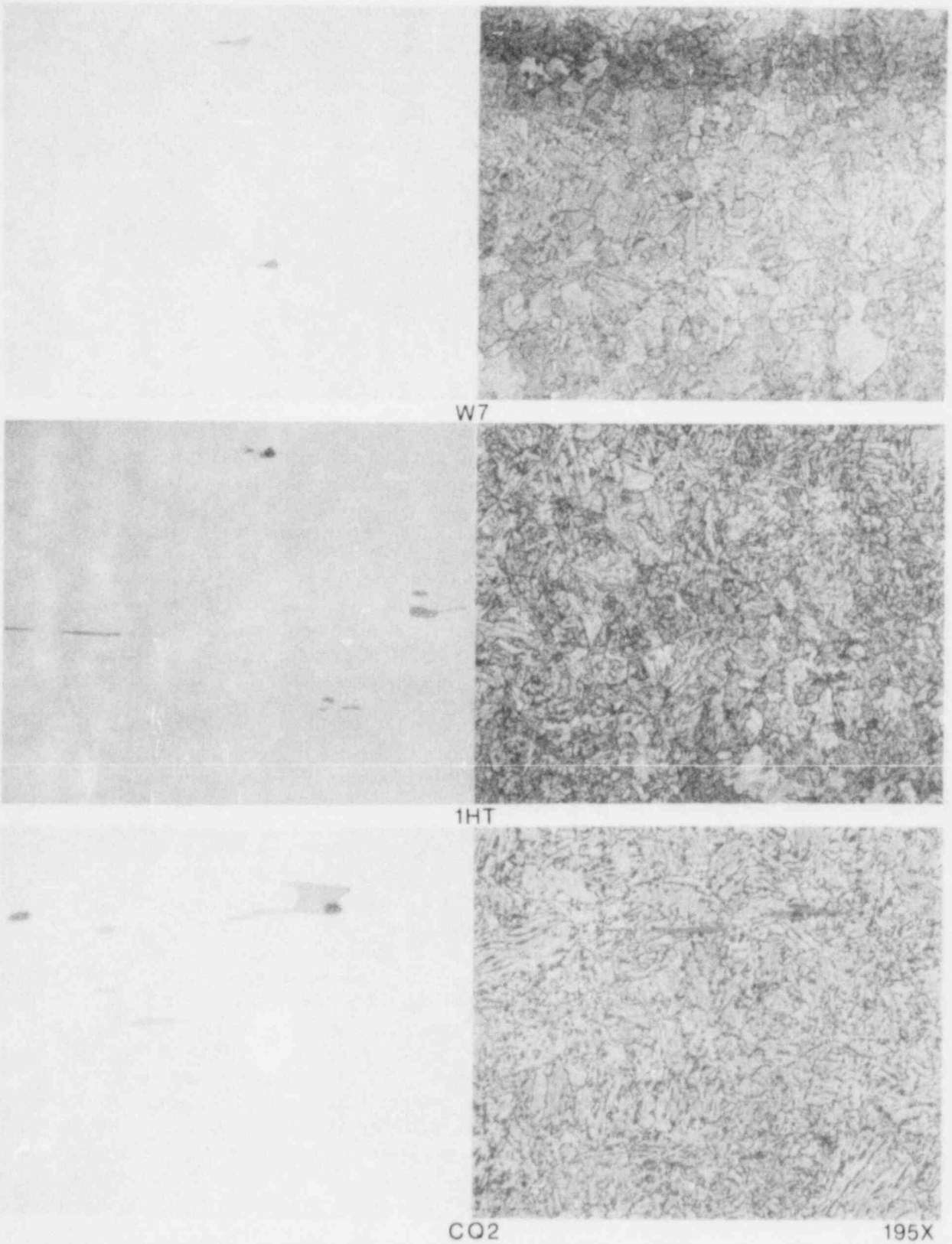

Fig. 9 The microstructures of the steels tested in this study. The left side is unpolished and shows the sulfide inclusion morphology. The micrographs on the right were prepared with a Nitol (4% nitric acid in methanol) etch.

Table 3 Results of MEA Water Analyses

	After Deionization	Mixed with B & Li	After Autoclaving
	(All in ppb, except as noted)		
Boron	0	995 ppm	1092 ppm
Lithium	0	0.95 ppm	1.3 ppm
Fluoride	<10	~10	45
Chloride	<10	75	150
Sulfate	2	15	110
Phosphate	8	12	180

These tests were carried out using constant load amplitude cycling, at a test frequency of 17 mHz and a load ratio (R) of 0.2. In accord with the test practice of earlier ICCGR round robins (Ref. 12), the initial ΔK was 27.5 MPa$\sqrt{m}$ (25 ksi$\sqrt{in.}$). The specimens were installed in the load train, placed in the autoclave which was filled with water, and brought to ~ 90°C for 12 to 14 hours to degas the water. The system was then pressurized and brought to 288°C (550°F). The cycling was initiated within 24 hours after the temperature was stabilized. In a departure from the usual MEA practice, but in agreement with the ICCGR methodology, the initial phase of this test was at 17 mHz.

The conduct of multiple specimen tests is somewhat different from the conduct of single specimen tests. In both cases, it is important to create a beachmark to accurately define the final crack length for each specimen tested. In the case of single-specimen tests, this is normally done by terminating the test, removing the specimen from the autoclave, chilling and fracturing the specimen. In the case of multiple-specimen tests, crack extension proceeds at different rates in different specimens, and thus the desired terminal crack length on individual specimens will be reached at different cyclic counts. In this case, when the first of the specimens reaches the final crack length, the loads (minimum and maximum) on the daisy chain of specimens are reduced to 50% of their original values, and the test frequency is increased to 1 Hz. Cycling is continued with these new parameters, until the specimen(s) with the longest crack lengths either break completely, or undergo significant crack extension. Crack extension on specimens with shorter cracks is generally very small or nonexistent. The test parameters are then returned to their original values, and the test continues on specimens remaining in the daisy chain.

At the conclusion of the series of tests, the autoclave is cooled and opened, the specimens removed and broken open, and the initial and final crack lengths, and any significant beachmarks in between are measured using micrometer-mounted optical microscopes. These

directly-measured crack lengths are used as input to a post-test correction procedure described in an earlier report (Ref. 13). This correction procedure not only takes into account changes in crack front morphology due to tunneling, but also corrects for any instrumentation errors which may have developed during these somewhat lengthy tests. Normally, deviations from compliance-calculated and optically-measured crack lengths are less than 1.5%. Macrophotographs of the specimens from the two multispecimen tests are shown in Fig. 10.

The crack length (a) vs. cyclic count (N) plots for the two daisy chains of specimens involved in this study are shown in Figs. 11 and 12. As can be seen, the CQ2 and 1HT specimens reached their final crack lengths after about 30000 cycles, at which time the loads were reduced and the frequency increased. In both tests, the two specimens either broke, or the cracks were extended, and the tests were resumed with the original test parameters. Additional test phases proceeded in much the same manner, until the last specimen had broken, and the autoclave was cooled and opened. It is important to note that this multiphase approach to fatigue crack growth testing does not appear to produce transient behavior in the crack growth rates. As seen in both Figs. 11 and 12 for the code W7 specimen, following each phase of reduced load and 1-Hz beachmarking, crack extension resumes immediately upon resumption of cycling at test loads. As shown below, crack growth rates recommence at their former values and increase smoothly from there.

4. RESULTS AND DISCUSSION OF CRACK GROWTH RATE STUDIES

Fatigue crack growth rate vs. applied ΔK plots are shown in Figs. 13 and 14 for the low and high flow rate tests. There is virtually no difference in crack growth rates for either the low, medium or high sulfur content steels in either flow rate case. The steels with the two highest sulfur contents (codes 1HT and CQ2) have roughly the same growth rates, while the low sulfur steel (code W7) exhibits substantially lower crack growth rates. The results for the remaining specimen in Fig. 13 (code W8B) which had 0.011% sulfur, reside somewhere in between the results for steels of lower and high sulfur contents, although this submerged-arc weld has a considerably different microstructure than the A 533-B plate specimens. These latter results are shown for completeness rather than because they lend support to the correlation between sulfur content and crack growth rates.

The fact that the results for the code W7 steel show little environmentally-induced acceleration eases the concern over whether the 100 to 200 ppb levels of sulfates, chlorides and other contaminents in the water have any effect on crack growth rates. A recent study by Van Der Sluys (Ref. 7) has shown that addition of 135 ppb chloride to an autoclave environment did not change crack growth rates. Scott has shown that addition of 1000 ppb sulfate ion as sulfuric acid does result in significant increases in crack growth rates. In spite of this observation, MEA is taking steps to install a water clean-up loop in its various autoclave systems.

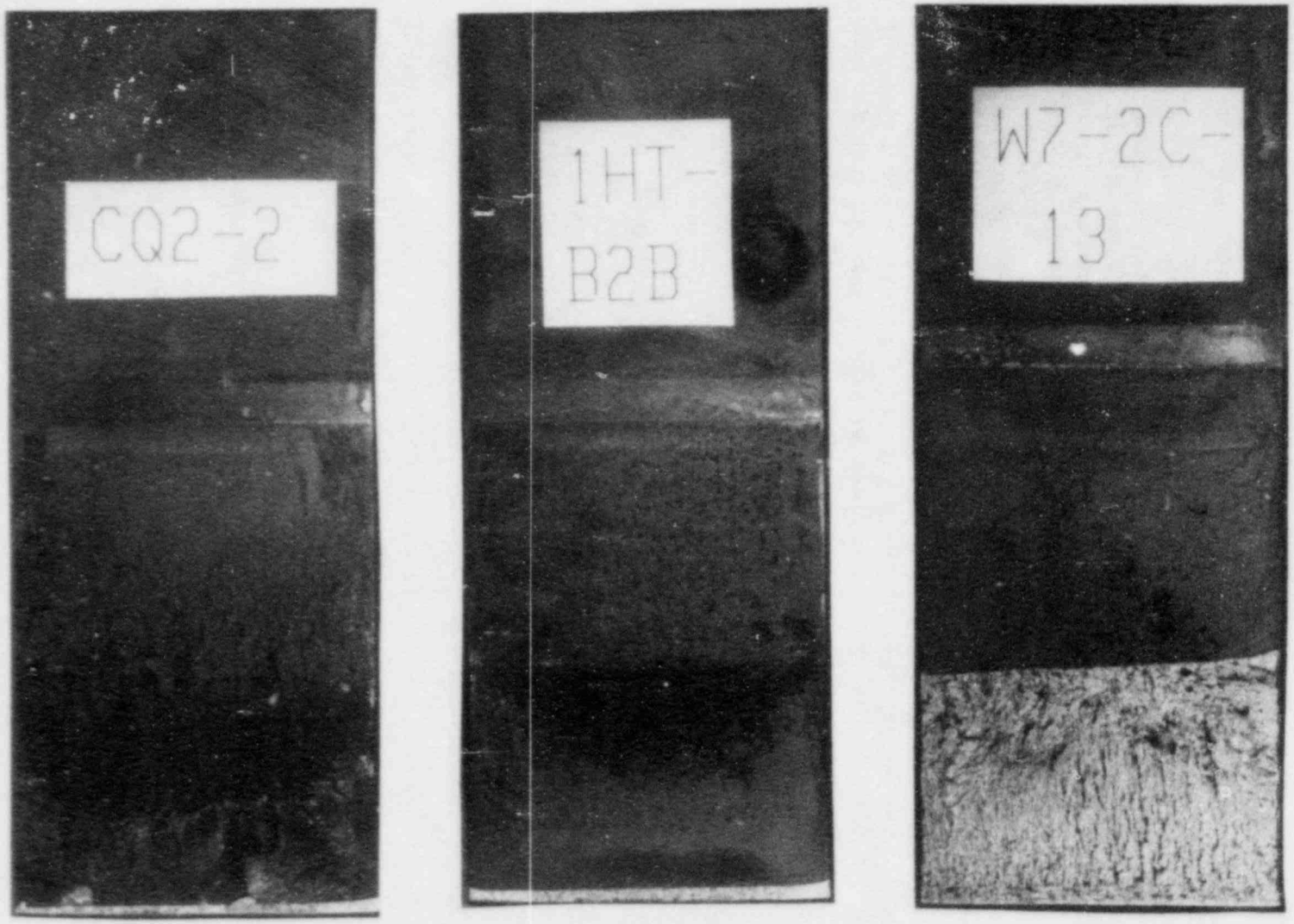
CQ2-2
1HT-
B2B
W7-2C-
13

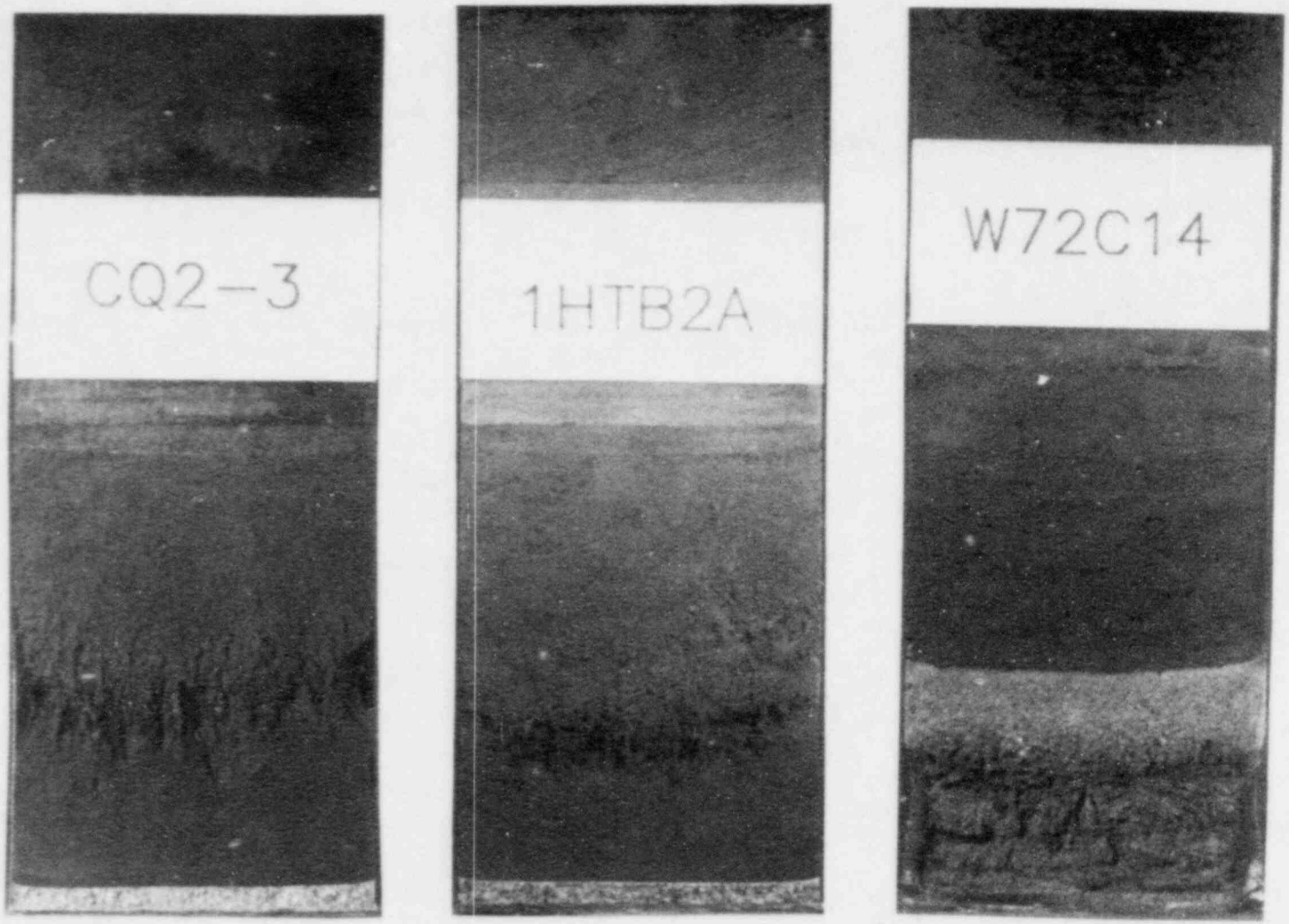

Fig. 10 Photographs of the fracture surfaces of the fatigue specimens showing the crack shape and beachmarks developed at changes in load and test frequency. Initial and final crack lengths are directly measured from the broken specimens.

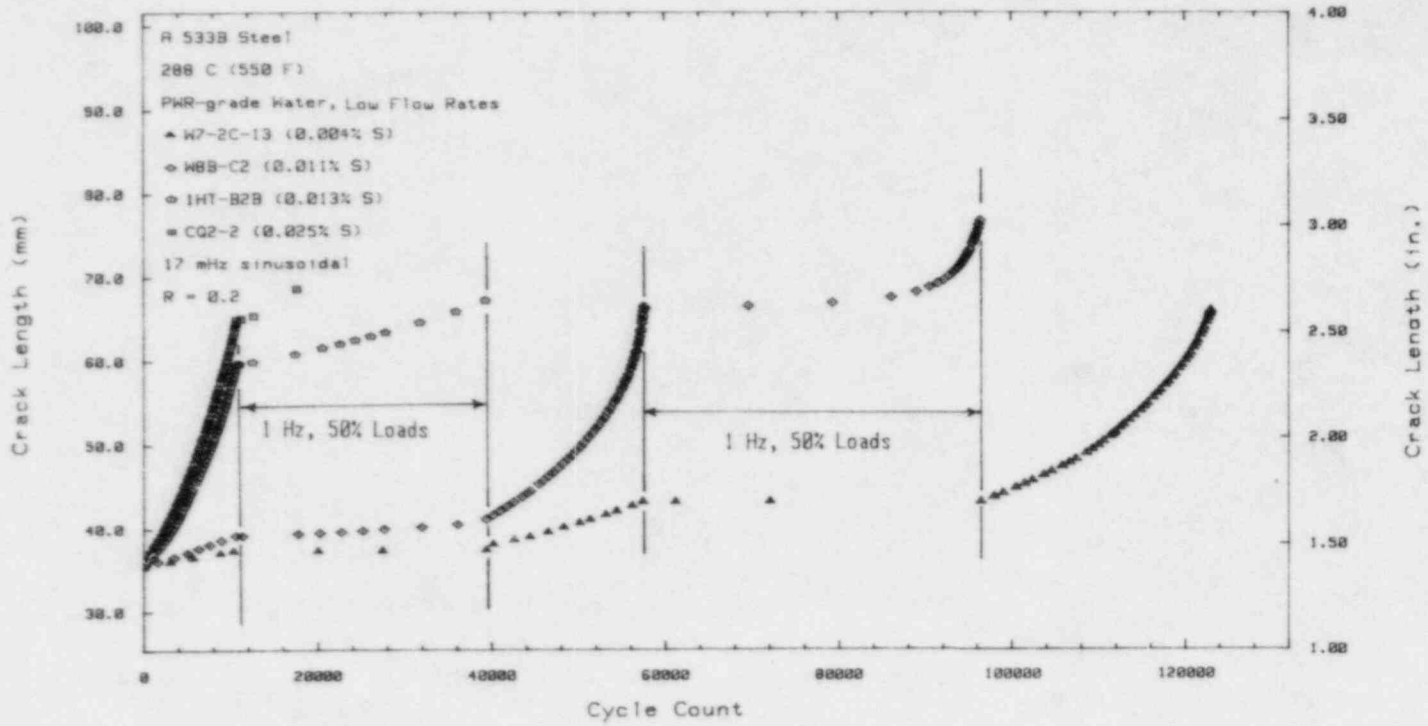

Fig. 11 Fatigue crack length vs. cyclic count for the specimens in the multispecimen test in the low flow rate environment.

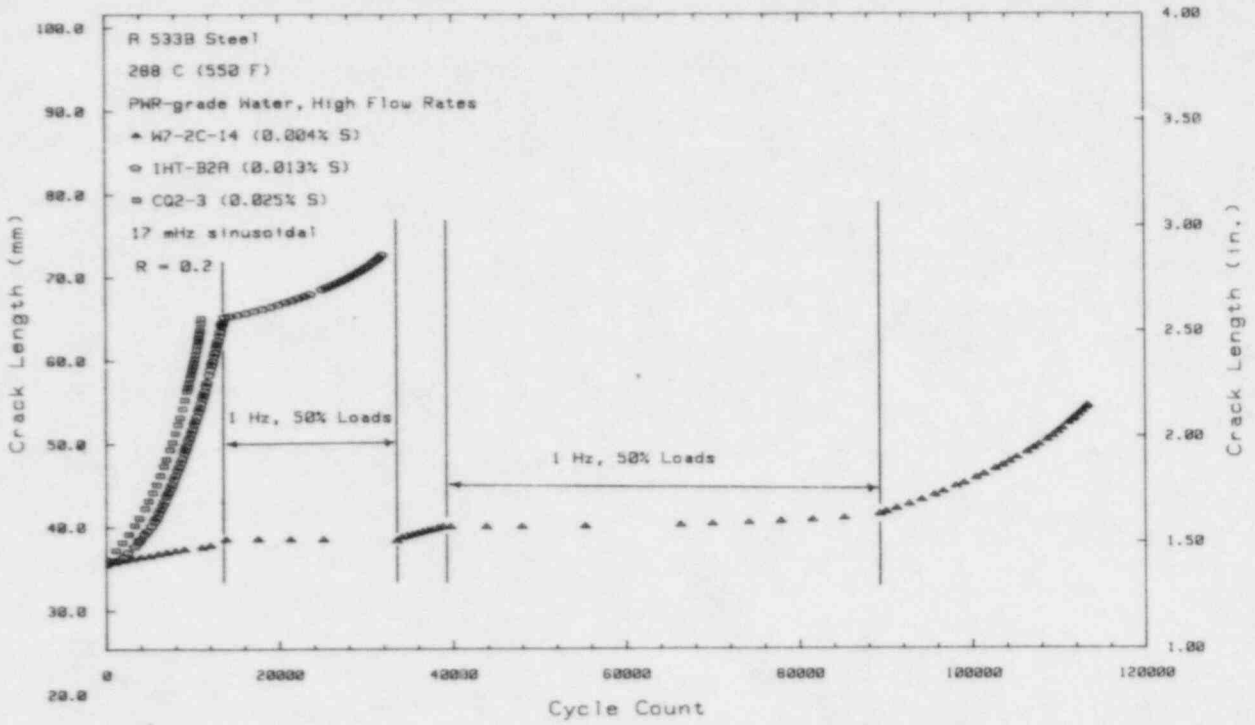

Fig. 12 Fatigue crack length vs. cyclic count for the specimens in the multispecimen test in the high flow rate environment.

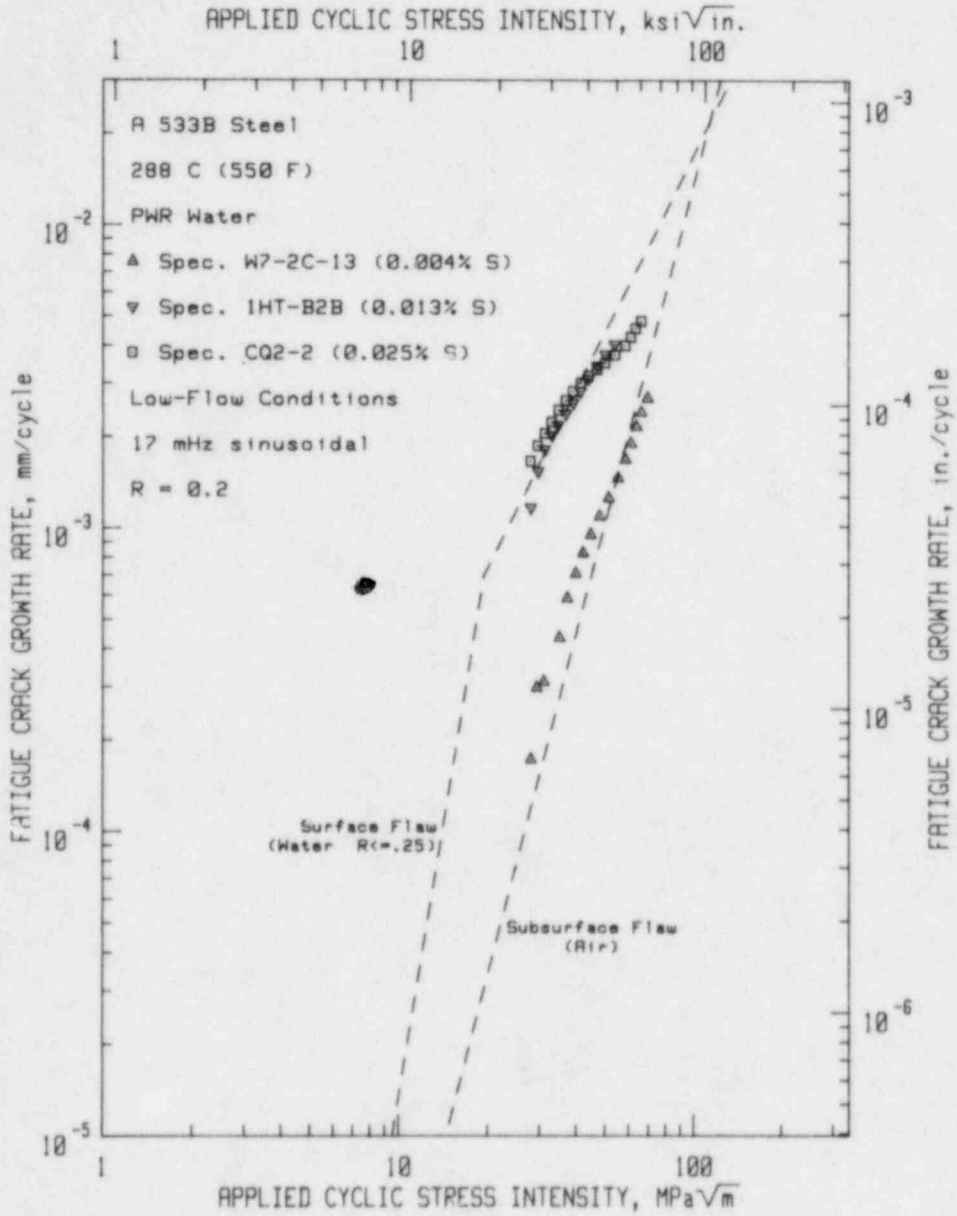

Fig. 13 Fatigue crack growth rates vs. applied cyclic ΔK for steels of varying sulfur contents and a load ratio of 0.2, tested in low flow rate environment. Test frequency was 17 mHz.

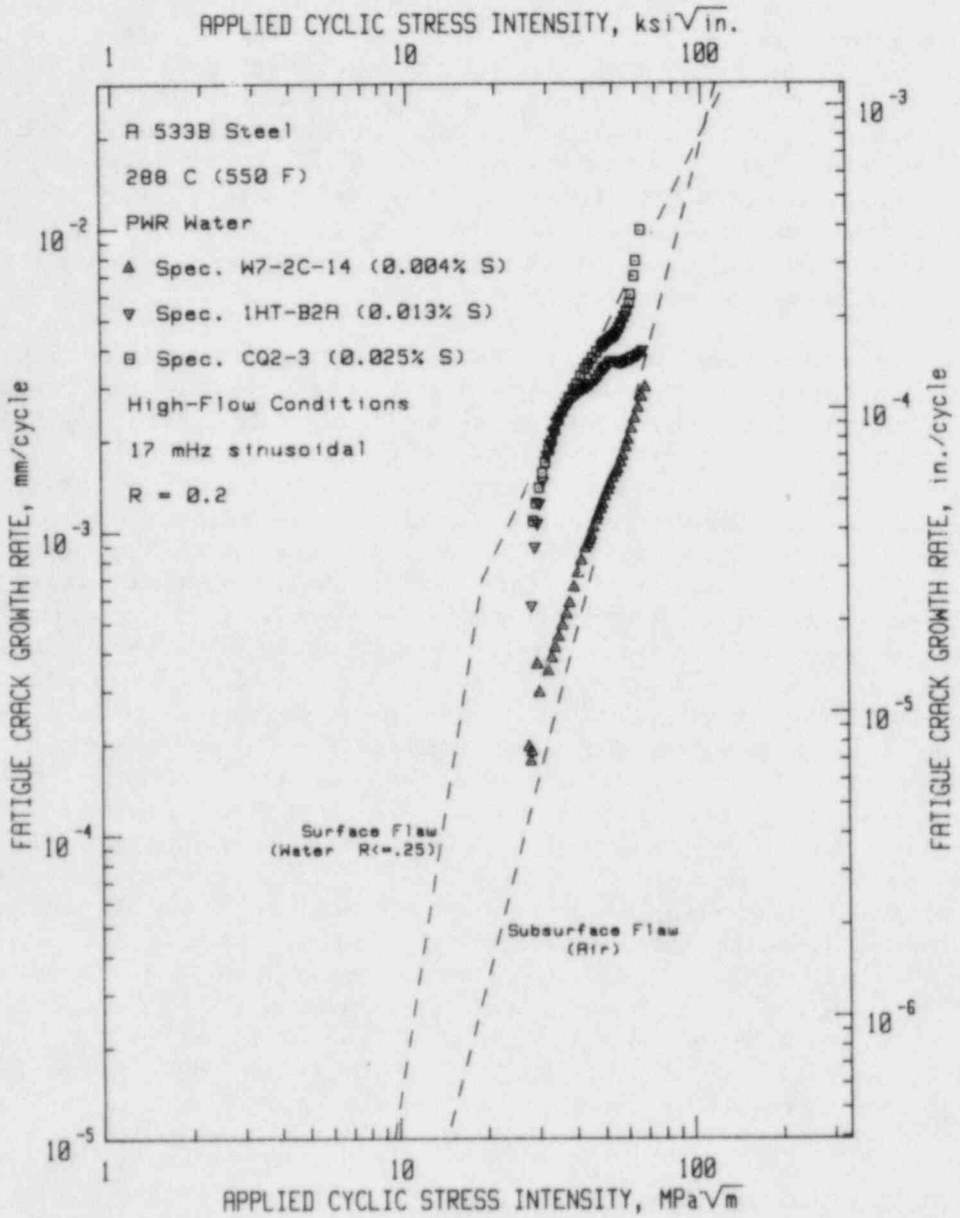

Fig. 14 Fatigue crack growth rates vs. applied cyclic ΔK for steels of varying sulfur contents and a load ratio of 0.2, tested in a high flow rate environment. Test frequency was 17 mHz.

The observations from the two multispecimen tests are straightforward. For a load ratio of 0.2 and a PWR environment, crack growth rates increase monotonically with sulfur content of the steels, while flow rate, over the range investigated, has no measureable effect. These results support the previous work on the effect of sulfur content, but are in contrast with the UKAEA results (Ref. 6), which show lower growth rates for steels covering the same range of sulfur contents. It is possible that the ultralow contaminent level in the autoclave water at the UKAEA test facility may have something to do with the lack of environmental assistance in the high sulfur content steels. This is tantamount to suggesting that it is some kind of twofold interaction of contaminents in the bulk water, together with sulfite/sulfate ion production within the crack tip enclave from solvating manganese sulfide inclusions which provides the conditions leading to the increase in crack growth rates.

Two other tests were conducted at a load ratio of 0.7 to determine if the sulfur contents of the code W7 and CQ2 steels (0.004% and 0.025%, respectively) provided the same relative levels of environmentally-assisted fatigue crack growth rates as at the lower load ratio. These tests were conducted in slowly flowing water, using constant amplitude loading, and the multispecimen test techniques described above. The fatigue crack growth rate vs. applied ΔK plots for these two tests are shown in Figs. 15a and 15b. These results show that there is virtually no difference in growth rates between the two steels, and that there is relatively little environmental assistance when compared to results published by Bamford (Refs. 3 to 5 and Fig. 4). Furthermore, in the case of the CQ2 specimen, fatigue crack growth rates during the 1-Hz phases of the test generally exceeded those growth rates during the 17-mHz phases. The test of the code W7 specimen involved such short crack extensions at the 1-Hz test frequency that growth rates cannot be accurately computed and a similar conclusion cannot be posed. This result is in general agreement with an earlier finding by Scott (Ref. 9), which indicated that in order to maximize the environmental-assistance component of fatigue crack growth in PWR environments, higher test frequencies were required at the higher load ratios. In the Scott research, test frequencies of 1 and 5 Hz at $R = 0.9$, 0.5 to 5 Hz at $R = 0.8$, and 1 to 20 Hz at $R = 0.7$ were required to produce a "plateau" in the growth rates, over which Scott postulated the corrosion process controlled the growth rates.

5. FRACTOGRAPHIC OBSERVATIONS

The specimens of the lowest and highest sulfur content steels (codes W7 and CQ2) from the $R = 0.2$ tests were examined to determine the fractographic features which characterized the environmentally-assisted fatigue crack morphology. As expected, when the environmental assistance was significant (in the CQ2 tests), the fatigue fracture surfaces are covered with brittle-appearing features, fan-shaped facets and extended areas covered with brittle striations, as shown in Figs. 16a and 16b. When the environmental assistance is low (as in the W7 tests), there is a mix of ductile- and brittle-striation formation, and overall, a much greater percentage of ductile appearing

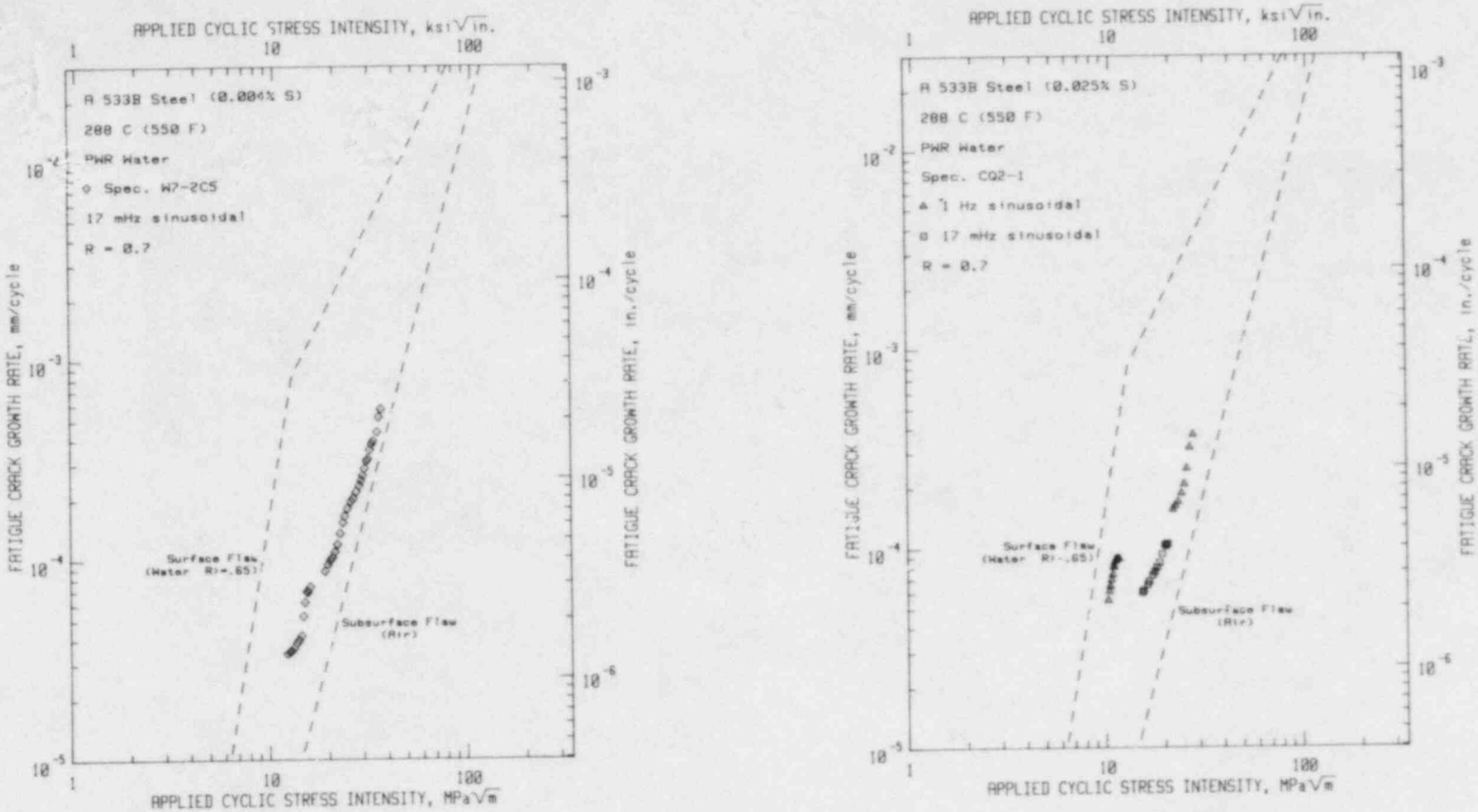

Fig. 15 Fatigue crack growth rates vs. applied cyclic ΔK for two steels of different sulfur contents and a load ratio of 0.7, tested in a low flow rate environment. Test frequency was 17 mHz. Some 1 Hz data points for the high sulfur steel (CQ2, Fig. 15a) show that growth rates are higher at the higher test frequency.

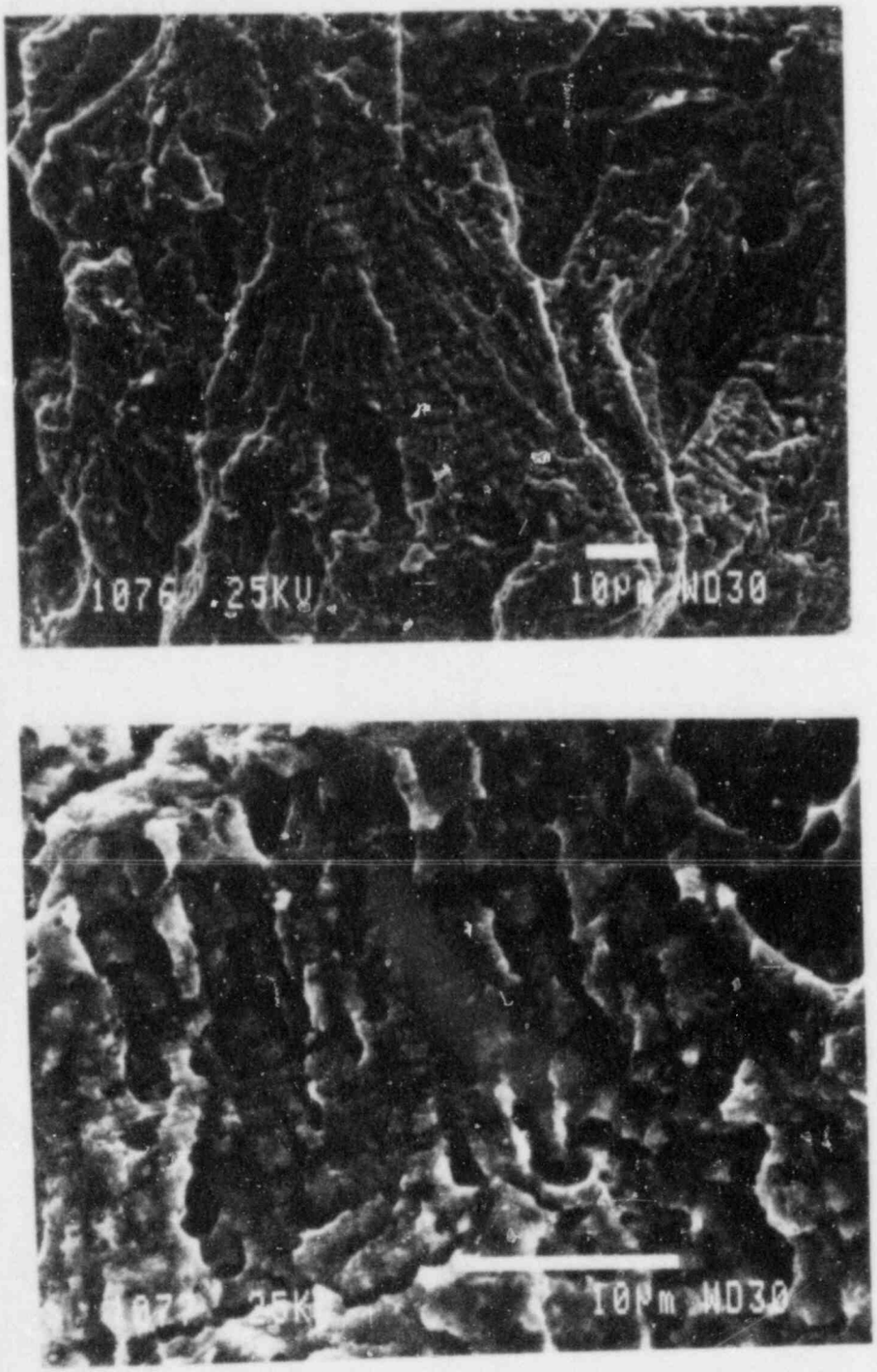

Fig. 16 Fractographic features of fatigue crack growth in the high sulfur steel showing the predominance of fan-shaped features and brittle striations usually associated with environmental assistance in these types of steels.

areas. An example of this morphology is shown in Fig. 17, showing that the ductile and brittle striations can be found within the same general area. Through comparison with Fig. 16, it can be seen that the brittle striations have the same appearance in both the high and low sulfur steels. These observations confirm earlier studies for similar crack growth rate tests (Ref. 14).

In spite of the significant difference in fracture surface appearance, metallographic cross-sections of the fracture surfaces on the two specimens show that there are no large differences in fracture surface roughness or transverse cracking. Overall, the surface is quite smooth in both cases.

These specimens did provide the opportunity to carry out some matching fracture surface observations, in which specific features which are micrographed on one face of the fatigue crack face, are matched in location on the opposite fatigue crack face, thus giving an indication of the way in which the fatigue crack faces fit together. Examples of matching fracture surface observations are shown in Figs. 18 and 19 for each of the two codes of specimens. In both cases, the match is essentially perfect, even down at the striation level, leading to the following conclusions:

- The ENDOX method of removing the oxide (Ref. 15) produced during crack extension in the PWR environment removes all of the oxide, and possibly some of the second-phase particles, but does not affect the metal matrix in any significant way.

- There is no significant plastic deformation which occurs on or under the fatigue fracture surface following formation of the crack. This implies that crack closure does not occur at this load ratio, and the crack-tip displacement (or stretch) is essentially nonexistent.

- Most importantly, from a micromechanistic point of view, there is no measureable dissolution of the ferrous matrix, as would be required by an anodic dissolution mechanism for environmentally-assisted crack growth.

Study of these fatigue fracture surfaces also provided a second important observation which relates to the mechanistic processes which control environmentally-assisted fatigue crack growth in these material and environment combinations. Figure 20 of the low sulfur steel, shows evidence of a nearly circular "burst" of crack opening, centered on what appears to be a small area of intergranular cracking. Figure 21 is an enlargement of the above figure showing that the match of features is perfect, and that there are no striations on this area, either ductile or brittle. Figures 22 and 23 show a similar area found on the high sulfur steel, with the burst centered on an inclusion site. Lastly, Fig. 24 shows a burst which was found in the volume ahead of the crack tip which was exposed when the specimen was chilled and fractured after completion of the fatigue crack growth test. This indicates that these areas were formed ahead of the actual

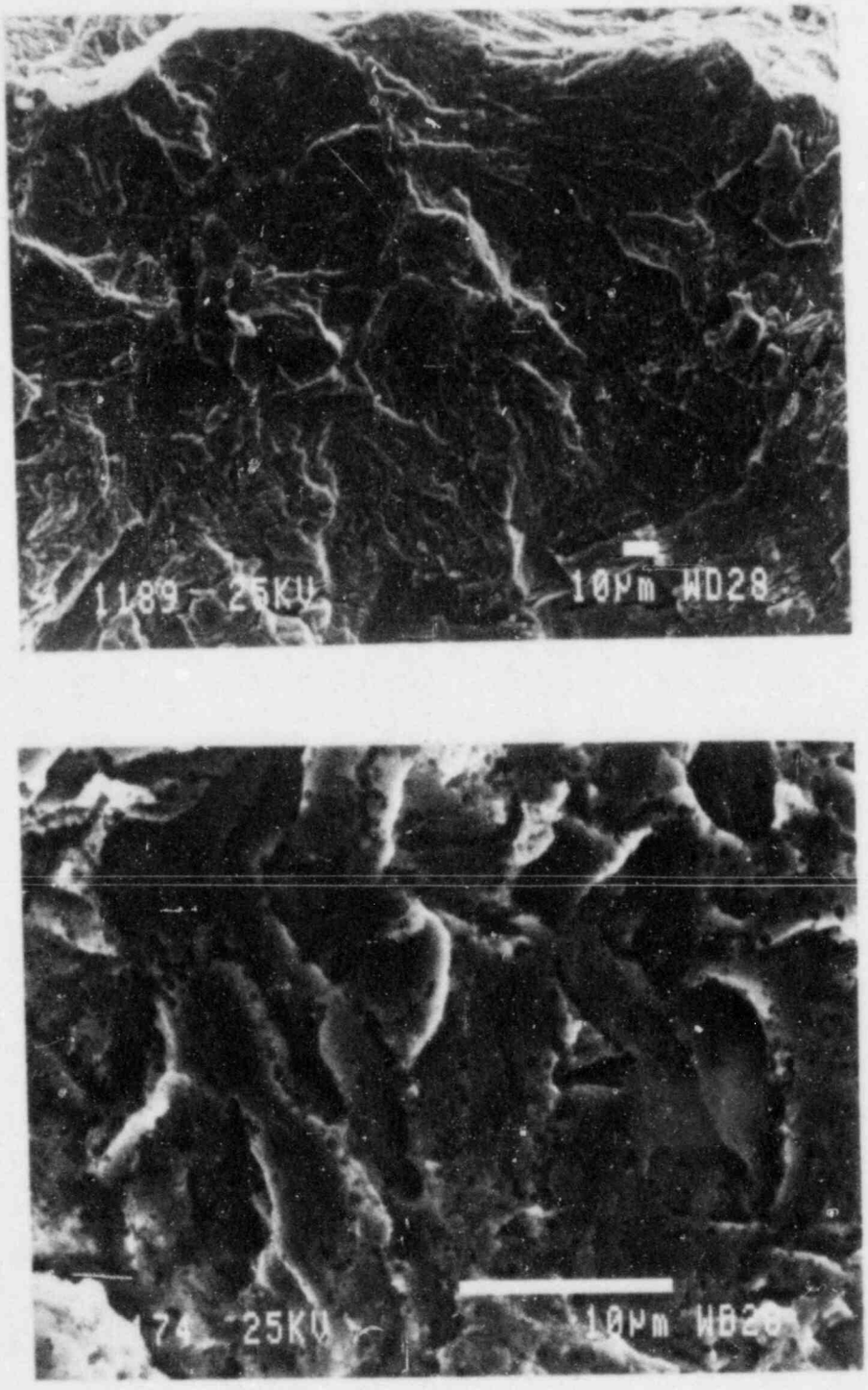

Fig. 17 Fractographic features of fatigue crack growth in the low sulfur steel showing a mix of features, both ductile and brittle in appearance.

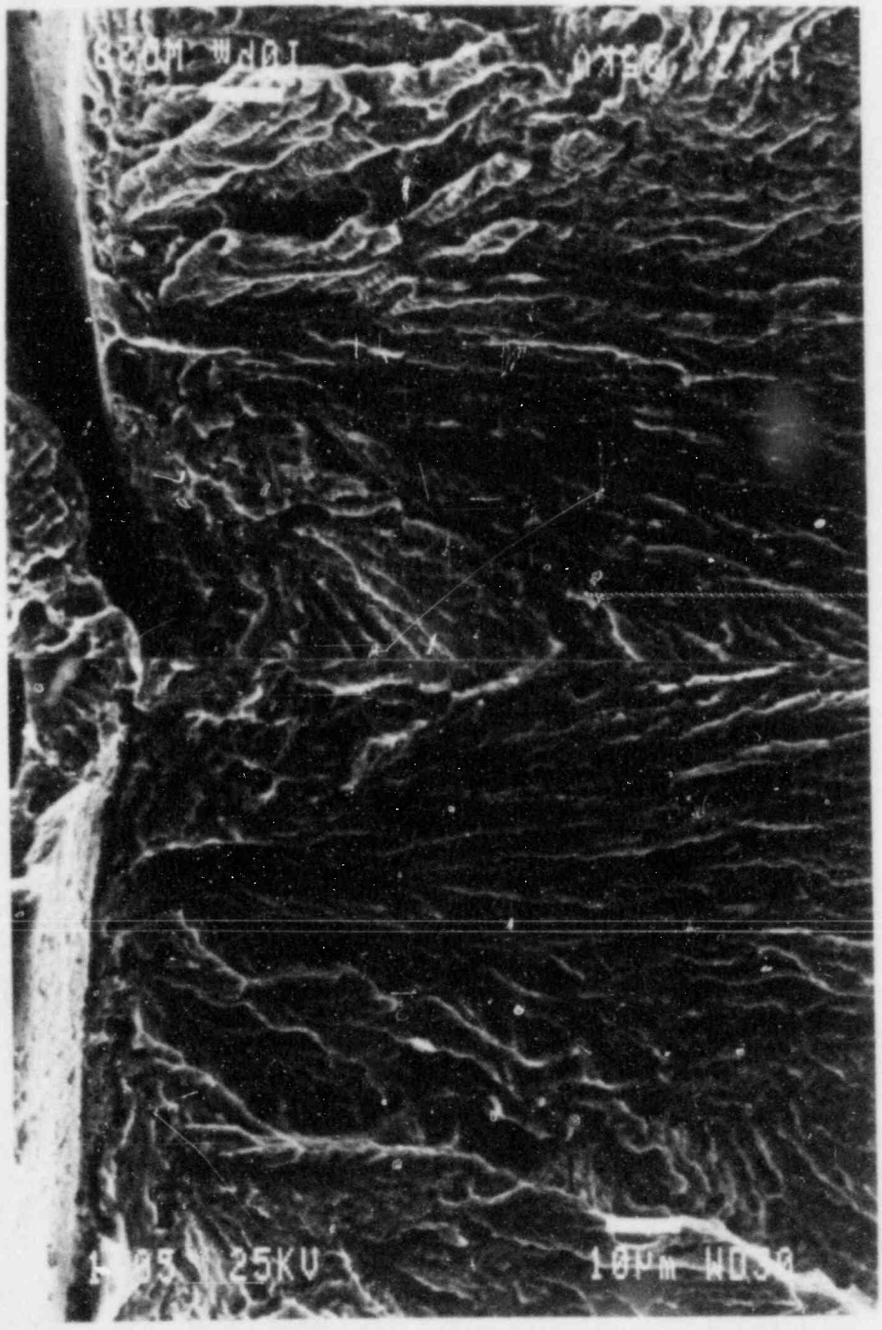

Fig. 18 SEM micrographs of matching fatigue fracture surfaces for the high sulfur steel specimen. The complementary match of the various features, is nearly perfect.

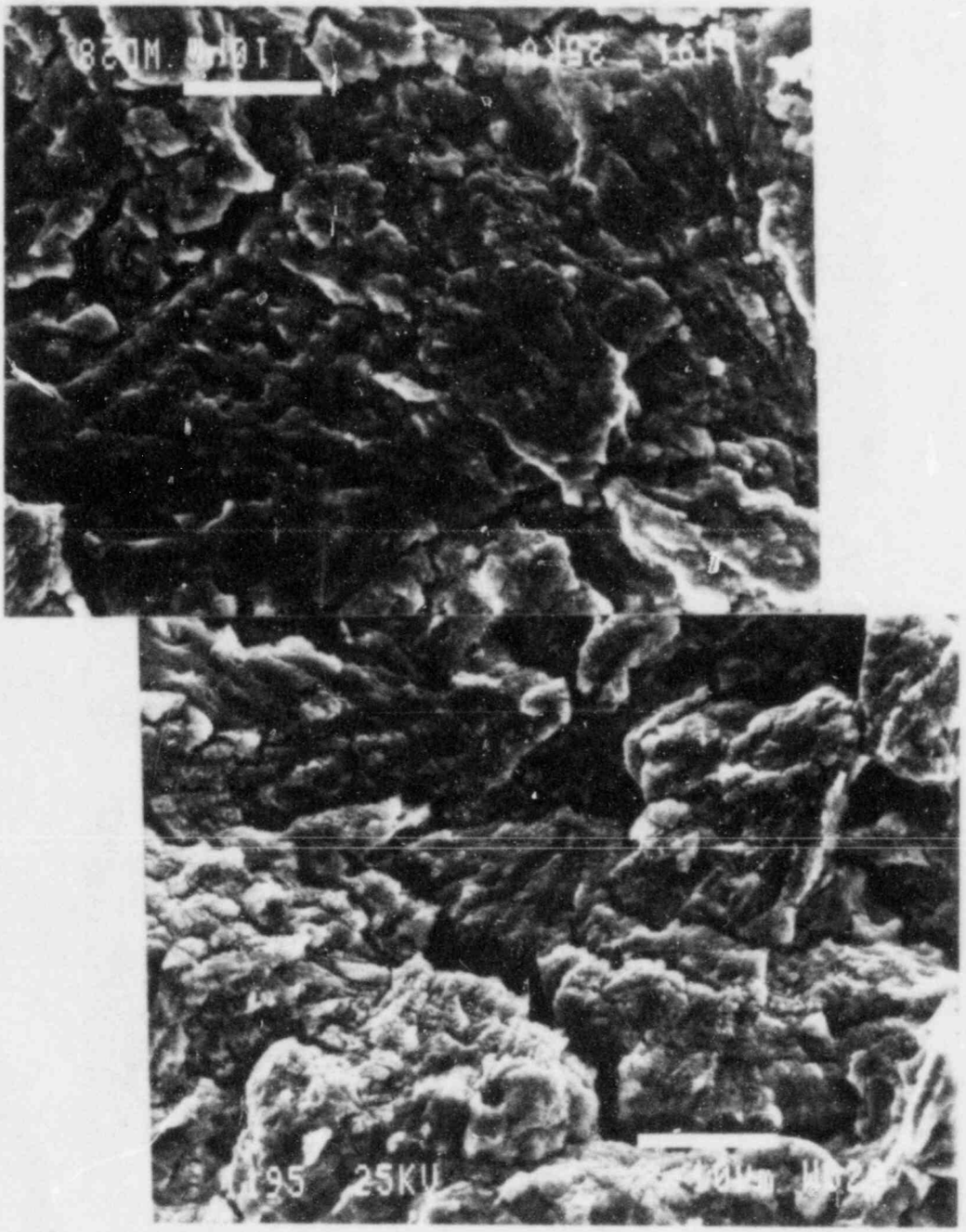

Fig. 19 SEM micrographs of matching fatigue surfaces for the low sulfur steel specimen. As above, the complementary match of the various features, is nearly perfect.

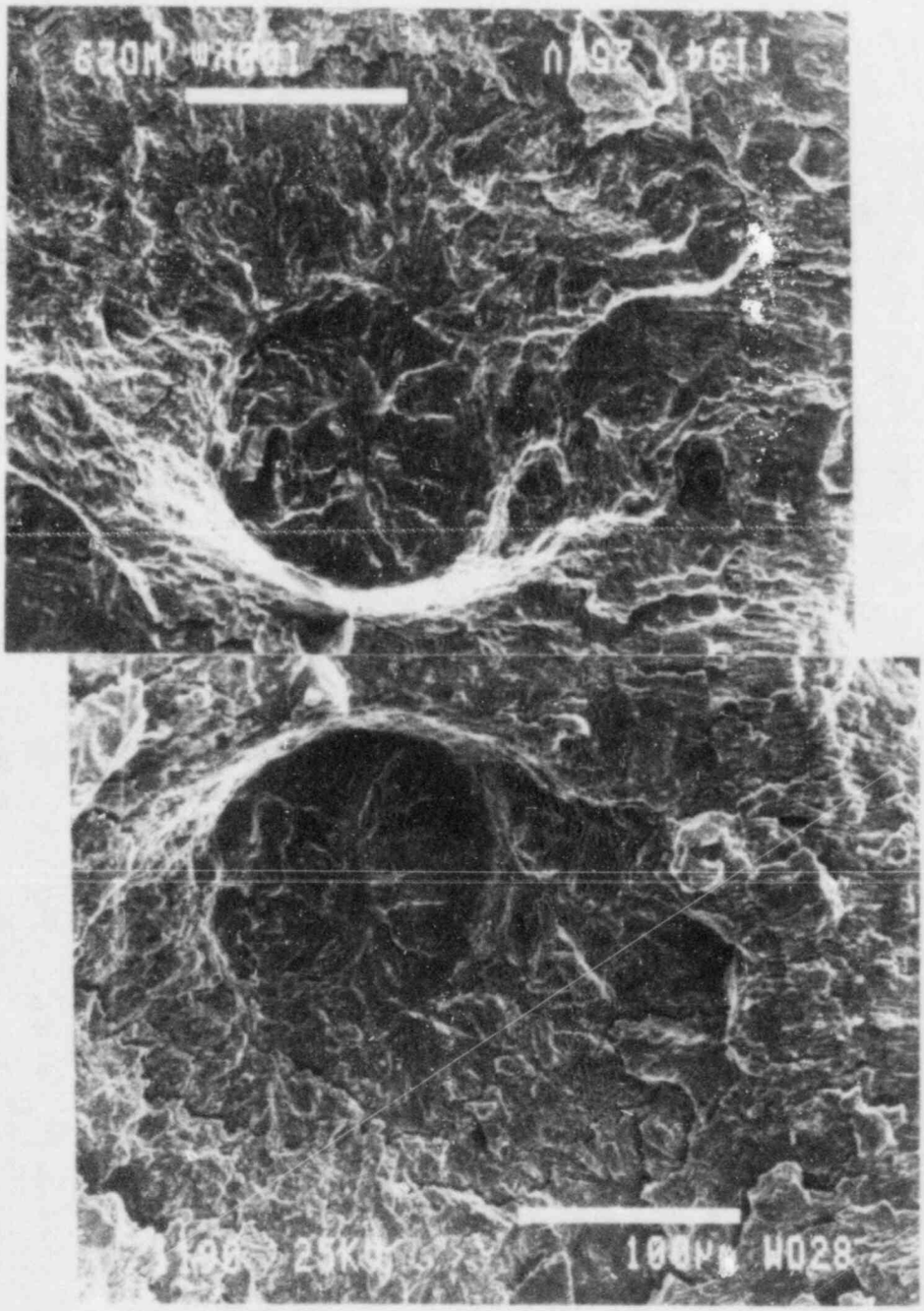

Fig. 20 Fractograph of a nearly circular area of brittle-like appearance and no evidence of striations or slow crack growth. This region, found on the low sulfur steel, is presumed to have formed by hydrogen cracking.

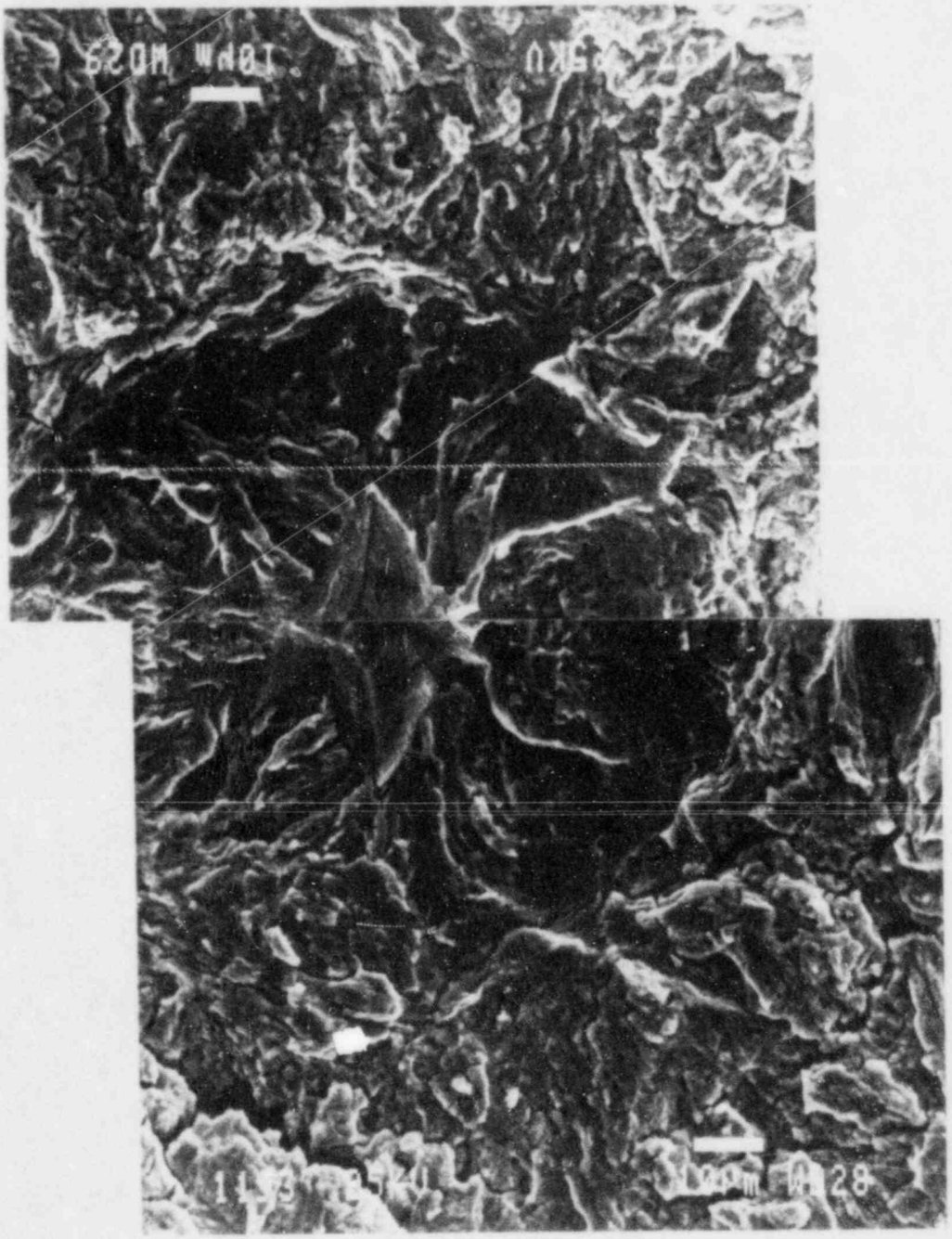

Fig. 21 Increased magnification and matching fracture surface view of the feature of the hydrogen cracking feature of Fig. 20. The match of features seems to be exact. This feature is centered on a small region of intergranular cracking.

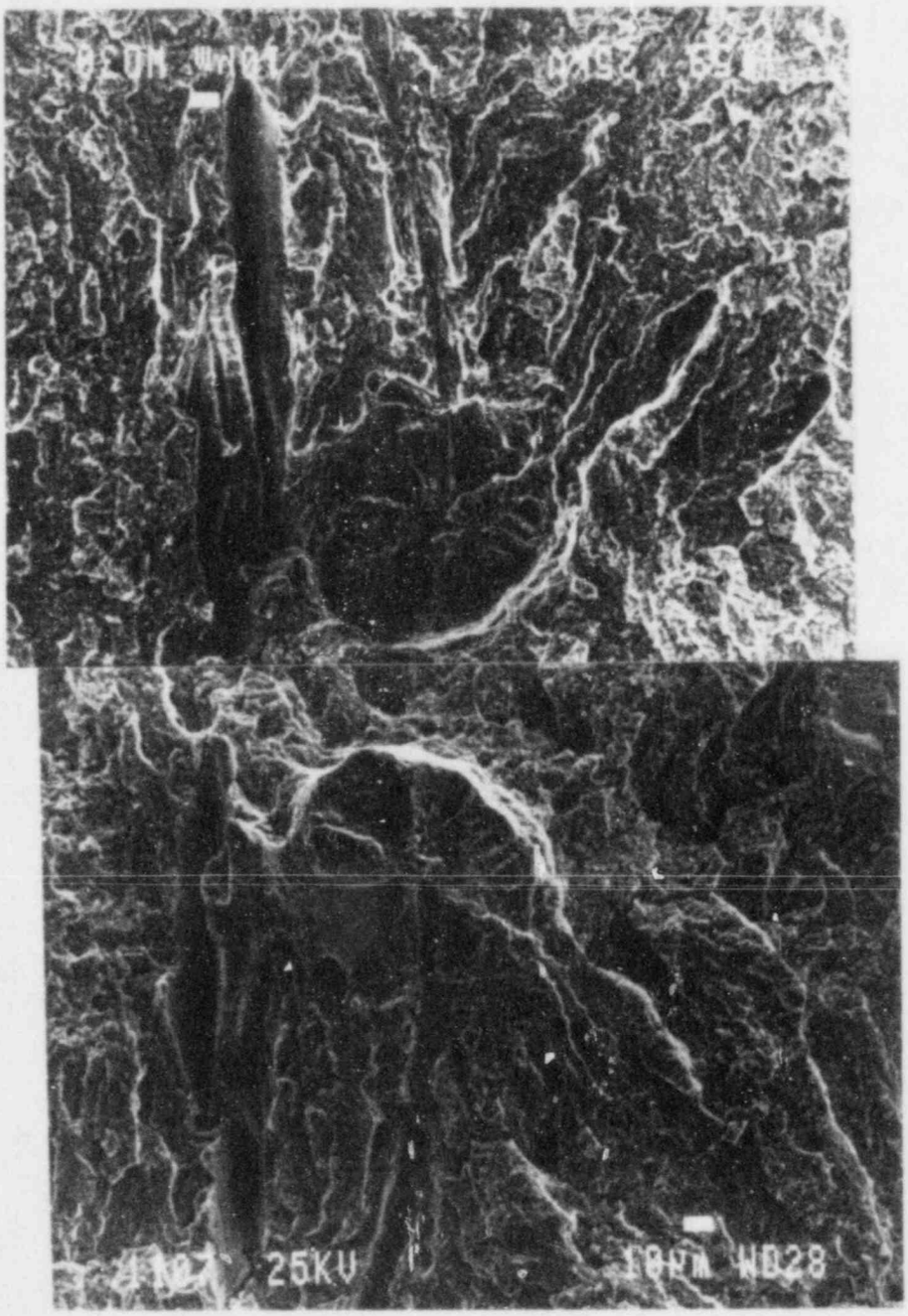

Fig. 22 Evidence of hydrogen cracking found in the high sulfur steel. This feature looks similar to that of Fig. 20, but the burst is centered on an inclusion site.

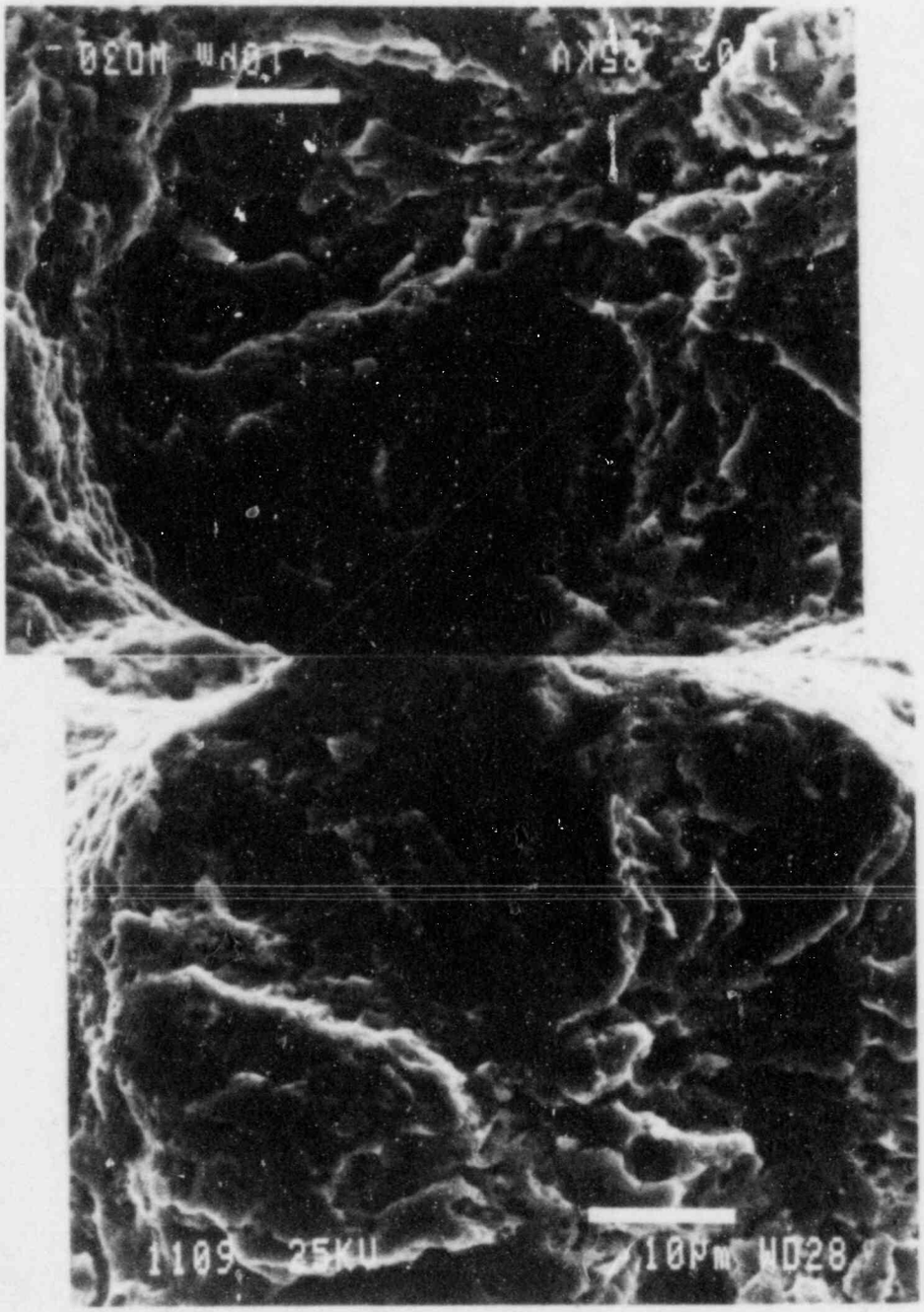

Fig. 23 Increased magnification and matching fracture surface view of Fig. 22.

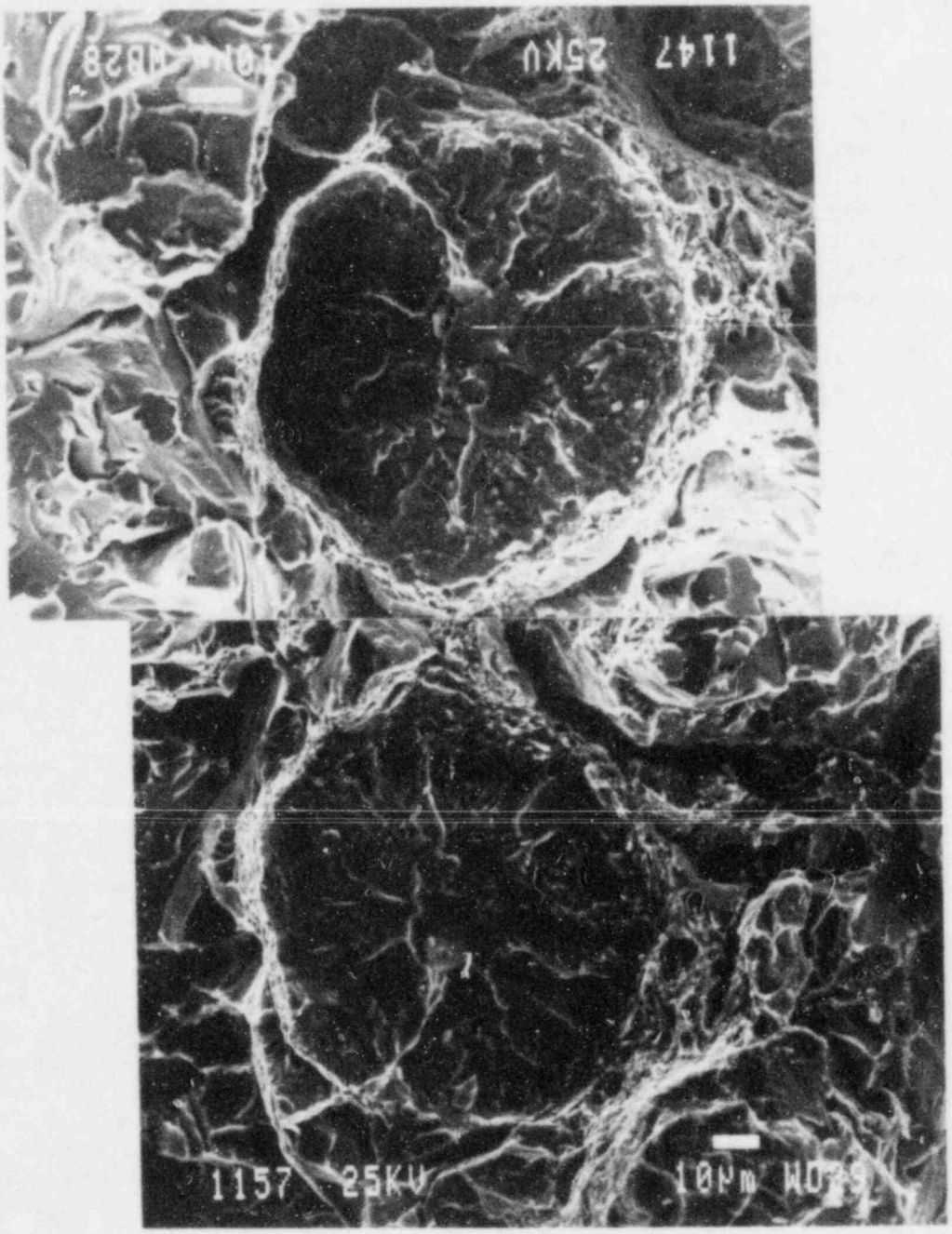

Fig. 24 A burst of hydrogen cracking located in the uncracked region ahead of the fatigue crack tip. This region was opened up during the post-test fracture of the chilled specimen. This is evidence that these areas formed in advance of the actual crack, and therefore are not caused by direct contact with the aqueous environment.

crack front, and so were formed in the absence of direct contact with the aqueous environment. For comparison purposes, Fig. 25 shows a similar burst which was formed during the tensile test of a hydrogen precharged pressure vessel steel, tested in an air environment. The likeness in appearance is striking, and extends even to a similar diameter of the burst.

Although an exhaustive inventory of the presence of these burst areas was not carried out for the two specimens, there were distinctly more of these on the low sulfur steel than on the high sulfur steel. The authors speculate that the lower number of overall inclusions in the cleaner code W7 steel leads to greater concentrations of hydrogen on the smaller number of inclusions, and thus a larger number of resultant hydrogen cracks.

From this observation, the authors postulate that hydrogen cracking, and hydrogen-assisted crack growth are the operative mechanisms accounting for the environmentally-assisted fatigue crack growth rates in pressure vessel steels, tested in pressurized, high temperature water of low oxygen content.

6. X-RAY PHOTOELECTRON SPECTROSCOPY (XPS) OBSERVATIONS

Two of the fatigue fracture surfaces, from the specimens of codes W7-2C-14 and CQ2-3, tested at high flow and R = 0.2, were examined using XPS techniques in order to determine the analysis of the surface oxide and the manner in which this analysis might change within the thickness of the oxide. Specimens were examined near the crack tip and on the flank of the crack closer to the initial crack length. The electron beam used in the XPS unit irradiates an area of about 25 mm^2, and so these results are typical of an overall, rather than a localized analysis. The procedure is to analyze the photoelectron spectrum from the solvent-cleaned, but otherwise as-received surface of the specimen, and then remove several nanometers of the oxide by inert-gas sputtering, and perform another analysis on the newly-exposed oxide surface. The process is repeated as desired, sometimes to the point of complete stripping of the surface oxide down to the bare metal. The irregular profile of the fatigue fracture surface causes nonuniform removal of the oxide, but for the relatively shallow depths, such as those studied for this report, the calculated sputtering depths are reasonably representative. The analyses are expressed in atomic percentage (a/0) of the individual elements, normalized to 100%, on the assumption that the five elements recorded were the essential constituents of the oxide layer. Inclusion of other elemental possibilities (Ni, Mn, P) would change slightly the actual numbers, but would not change the relative amounts of the cited elements.

The results of the composition analysis of oxide at various depths, as measured from the surface, are presented in Table 4. Magnetite (Fe_3O_4) is the predominant oxide phase, as has been demonstrated previously (Ref. 16). Intuition suggests that the analysis of W7-2C-14 near the crack tip (#4 in the table) should be most

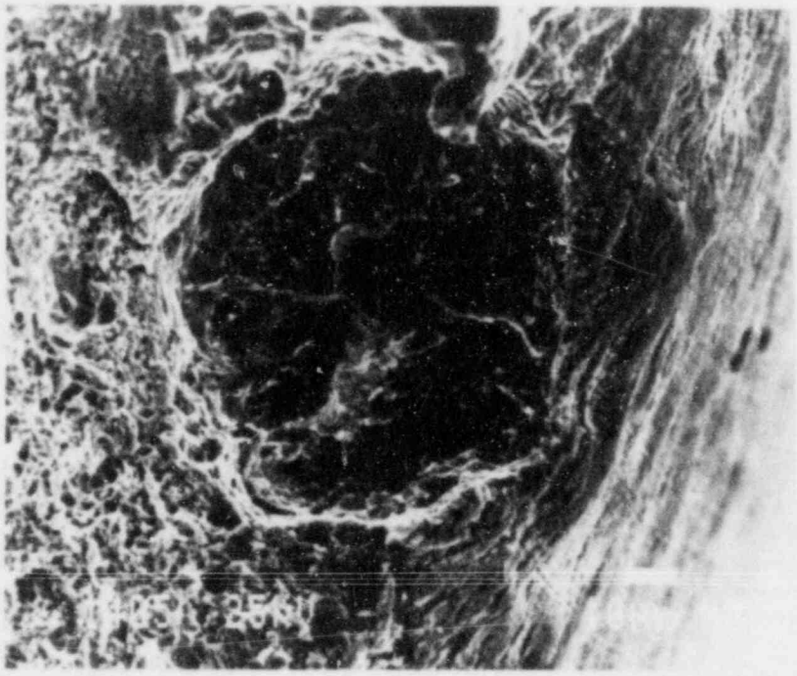

Fig. 25 Example of burst formation found on fracture surface of a hydrogen-charged tensile specimen. This feature is nearly identical, in shape and size, with the burst features found on the fatigue fracture surface shown in Figs. 20 through 23.

representative of the situation near a growing crack tip, since the test was terminated and the specimens removed from the autoclave shortly after this area developed. However, the two analyses (near crack tip and on the flank) from each of the two specimens are remarkably similar, and the initial crack length analysis from W7 and the crack tip analysis from CQ2 (#2 and #3) should be comparable because they were exposed to the water for about the same amount of time. The analysis of the CQ2 oxide on the flank near the initial crack length (#1) holds the least credibility, especially near the surface, because of the long postfailure residence in the autoclave environment.

Table 4 Composition of Fatigue Fracture Surfaces (at-%) After Various Sputtering Times

Sample	Distance from Original Surface (nanometers)	Fe	Cl	S	O	C
CQ-2-3						
#1 Near	0	4.6	0	0	22.7	72.7
Initial	5	---	---	---	----	----
Crack	25	21.6	1.7	1.9	27.5	47.4
	45	24.2	1.9	3.2	41.1	29.7
#2 Near	0	4.8	0.9	0	18.3	76.7
Crack	5	15.4	1.5	1.4	38.4	43.3
Tip	25	18.4	1.5	1.3	40.1	38.6
	45	18.1	1.6	1.2	45.7	33.4
W7-2C-14						
#3 Near	0	1.9	0.6	0.7	24.0	72.7
Initial	5	16.7	1.5	2.3	43.3	36.2
Crack	25	23.9	2.5	2.4	42.6	28.7
	45	23.6	3.9	4.1	41.7	26.8
#4 Near	0	2.0	0.5	1.0	22.3	74.3
Crack	5	---	---	---	----	----
Tip	25	15.6	1.9	1.5	24.8	56.8
	45	18.2	3.9	4.9	35.1	37.8

The large percentage of carbon cannot be considered valid within the present study. The specimens were corrosion-protected with an oil-based anticorrodent, which was subsequently removed, just before the XPS observations, with methyl-ethyl-ketone solvent. Thus, there may

have been large amounts of hydrocarbon residues which had infiltrated the oxide layer between test termination and XPS studies.

The fact that the sulfur content of the W7 oxide is two to four times greater than that of the CQ2 oxide, exactly opposite of the chemistry of the steels themselves, is interesting, but inexplicable by these authors. There is a strong gradient of sulfur concentration with depth, approaching zero at the surface, indicating that the sulfur must occur in some soluble form. The 1.5 a/0 to 3.9 a/0 of chlorine found in the oxide subsurface does indicate that the chloride does participate in the oxide formation in some way. There is a correlation between the sulfur and chlorine levels for each of the two specimens: CQ2 having lower sulfur and chlorine, and W7 having higher sulfur and chlorine. It is not likely that the lower levels of these two elements on CQ2 are due to dissolving of the species in autoclave water while the crack was open following the early failure of the specimen, because analyses #3 from W7 and #4 from CQ2 should represent oxides formed at roughly the same time, and because analyses #3 and #4 from W7 represent vastly different times of exposure to the autoclave environment, and yet are remarkably similar in the quantities of elements, and their gradients with depth.

The spectra which emerge from an XPS analysis reflect not only the amounts of individual elemental species, but also the electronic binding energies of the valence electrons. This information can be combined with the peak height and real analyses to get some information on the elemental compounds and their relative proportions. An example of the peak structure for the initial crack area on the low sulfur specimen (W7), is shown in Fig. 26. The binding energies of the $Fe_2p^{3/2}$ electrons for the compounds Fe_3O_4, FeS and FeS_2 are shown on the figure. A peak centered on a particular value of binding energy indicates presence of that particular compound. On the outside surface of the oxide, magnetite is the only prevalent specie. However, as the oxide is sputtered away to reveal the deeper constituents, strong peaks for both FeS and FeS_2 emerge, while the peak for Fe_3O_4 recedes somewhat. This is an important finding, for it confirms the Pourbaix diagram for the Fe-S-H_2O system, which indicates that both compounds should exist for deoxygenated water, of near-neutral pH and cathodic potentials. Conversely, both compounds would not exist if the potentials were anodic or the crack tip environment were characterized by a low pH (acidic).

7. CONCLUSIONS

On the basis of this study, involving multispecimen testing, at two different flow rates, post-test metallographic and fractographic analyses and X-ray photoelectron spectroscopy of selected specimens, the following conclusions can be drawn:

- Crack growth rates have a strong dependence on sulfur content, with the caveat that the shape of the sulfide inclusion may have an influence on the degree of environmental assistance.

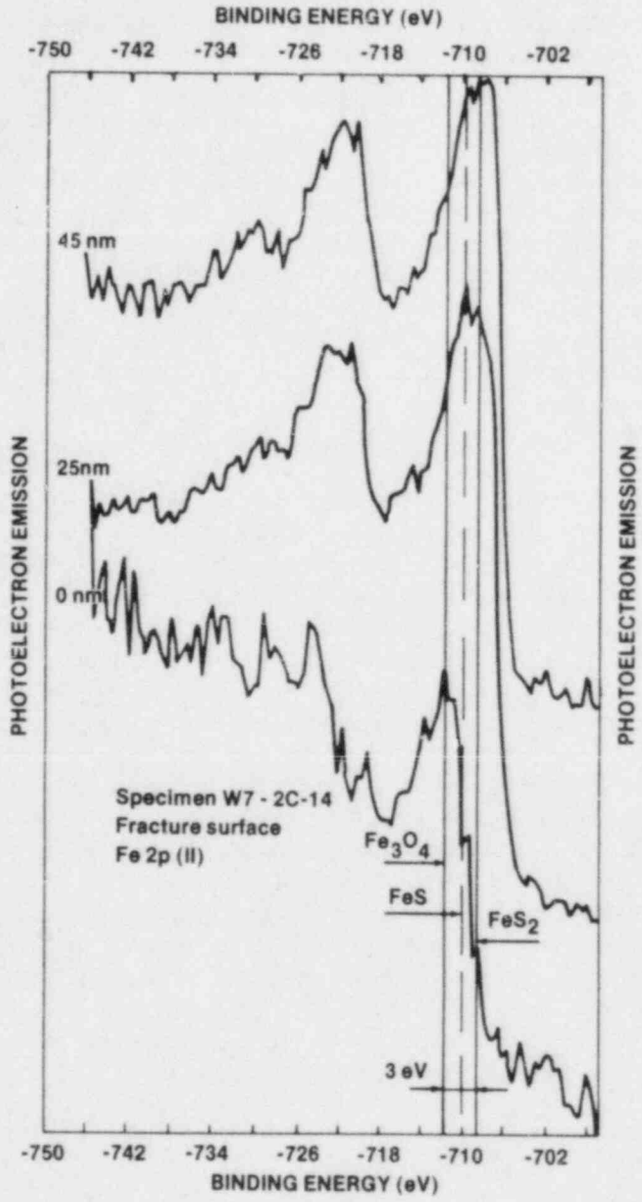

Fig. 26 X-ray photoelectron spectra for the $Fe_2p^{3/2}$ electron binding energy. The peaks for the FeS and FeS_2 compounds at 25 nm and 45 nm suggest the coexistence of these two species at the subsurface of the oxide.

- The flow rate of the environment in the vicinity of the specimens seems to have little effect on the crack growth rates.

- The fractography can be characterized as follows:

  a. The high sulfur steel exhibited brittle-like features, including fan-shaped facets and brittle striations over the entire fatigue fracture surface.

  b. The low sulfur steel exhibited a combination of brittle-like and ductile features, often residing side-by-side.

  c. Evidence of pure hydrogen cracking could be found on specimens from both heats of steel, although the low sulfur steel appeared to have more of these "bursts."

  d. The fractographic features match perfectly on both sides of the fatigue fracture face. This indicates that there is little, if any, dissolution of metal species at the crack tip or along the flanks of the crack.

- The XPS analyses of the oxides on the flanks of the crack show that chlorine and sulfur are incorporated into the oxides, and that both FeS and FeS_2 are present. As determined in previous tests (Ref. 16), the oxide phase is magnetite Fe_3O_4. These facts indicate that cathodic potentials and near-neutral pH conditions are obtained at the crack tip.

REFERENCES

1. G. Slama and P. Rabbe, "French Approach and Results in Cyclic Crack Growth," Proceedings of the 5th SMIRT Post-Conference Seminar, Paris, France, Aug. 1981, pp. 311-325.

2. "Standard Test Method for Plane-Strain Fracture Toughness of Metallic Materials," Designation E 399-83, in 1983 Annual Book of ASTM Standards - Metals Test Methods and Analytical Procedures, Section 3, Vol. 03.01, revised annually, American Society for Testing and Materials, Philadelphia, PA, 1983, pp. 518-553.

3. W. H. Bamford, "Environmentally Assisted Crack Growth Studies," in Heavy Section Steel Technology Report for October-December 1982, USNRC Report NUREG/CR-2751, Vol. 4, May 1983, pp. 139-161.

4. W. H. Bamford and L. J. Ceschini, "Environmentally Assisted Crack Growth Studies," in Heavy Section Technology Report for April-June 1983, USNRC Report NUREG/CR-3334, Vol. 2, December 1983, pp. 104-115.

5. W. H. Bamford, L. J. Ceschini and R. J. Jacko, "Environmentally Assisted Crack Growth Studies," in Heavy Section Steel Technology Report for July-September 1983, USNRC Report NUREG/CR-3334, Vol. 3, March 1984, pp. 97-114.

6. P. M. Scott, A. E. Truswell and S. G. Druce, "Corrosion Fatigue of Pressure Vessel Steels in PWR Environments - Influence of Steel Sulfur Content," Corrosion, Vol. 40(7), 1984, pp. 350-357.

7. "Corrosion Fatigue Characterization of Reactor Pressure Vessel Steels," Progress Report, October 1, 1982 to April 30, 1983, Project 1325-1, A. Van Der Sluys, Principal Investigator, Babcock & Wilcox, available from R. L. Jones, Electric Power Research Institute, Palo Alto, CA, July 1983.

8. Section XI of the ASME Boiler and Pressure Vessel Code, Rules for In-Service Inspection of Nuclear Power Plant Components, ANSI/ASME-BPV-XI-1, American Society of Mechanical Engineers, New York, issued annually.

9. P. M. Scott and A. E. Truswell, "Corrosion Fatigue Crack Growth in Reactor Pressure Vessel Steels in PWR Primary Water," Journal of Pressure Vessel Technology, Vol. 105, 1983, pp. 245-254.

10. W. H. Cullen, et al., "Operation of a High-Temperature, Pressurized Water Fatigue Crack Growth System," Closed Loop Magazine, October 1980, pp. 3-14.

11. W. H. Cullen, et al., "A Computerized Data Acquisition System for a High-Temperature, Pressurized Water Fatigue Test Facility, in Computer Automation of Materials Testing, ASTM STP 710, American Society for Testing and Materials, Philadelphia, PA, 1980, pp. 127-140.

12. R. L. Jones, "Cyclic Crack Growth in High-Temperature Water - Results of an International Testing Round Robin," in Proceedings of the International Atomic Energy Agency Specialists Meeting on Subcritical Crack Growth - Sessions I and II, USNRC Report NUREG/CP-0044, MEA-2014, Vol. 1, May 1983, pp. 65-88.

13. W. H. Cullen, et al., "The Temperature Dependence of Fatigue Crack Growth Rates of A 351 CF8A Cast Stainless Steel in LWR Environment," USNRC Report NUREG/CR-3546, April 1984.

14. W. H. Cullen, et al., "Fatigue Crack Growth of A 508-2 Steel in High-Temperature, Pressurized Reactor-Grade Water," USNRC Report NUREG/CR-0969, September 1979.

15. P. Yuzawich and C. W. Hughes, "An Improved Technique for Removal of Oxide Scale from Fractured Surfaces of Ferrous Materials," Practical Metallography, Vol. 15, 1978, pp. 184-195.

16. W. H. Cullen, K. Torronen and M. Kemppainen, "Effects of Temperature on Fatigue Crack Growth of A 508-2 Steel in LWR Environment," USNRC Report NUREG/CR-2013, April 1983.

NRC FORM 335 (11-81)

U.S. NUCLEAR REGULATORY COMMISSION

BIBLIOGRAPHIC DATA SHEET

1. REPORT NUMBER (Assigned by DDC)
NUREG/CR-4121
MEA-2053

4. TITLE AND SUBTITLE (Add Volume No., if appropriate)
The Effects of Sulfur Chemistry and Flow Rate On Fatigue Crack Growth Rates in LWR Environments

2. (Leave blank)

3. RECIPIENT'S ACCESSION NO.

7. AUTHOR(S)
W. H. Cullen/MEA
M. Kemppainen, H. Hanninen and K. Torronen/TRC

5. DATE REPORT COMPLETED
MONTH: January YEAR: 1985

9. PERFORMING ORGANIZATION NAME AND MAILING ADDRESS (Include Zip Code)
Materials Engineering Associates, Inc.
9700-B George Palmer Highway
Lanham, Maryland 20706-1837
Technical Research Centre of Finland, Vuorimiehentie 5
SF-02150 Espoo 15, Finland

DATE REPORT ISSUED
MONTH: February YEAR: 1985

6. (Leave blank)

8. (Leave blank)

12. SPONSORING ORGANIZATION NAME AND MAILING ADDRESS (Include Zip Code)
Division of Engineering Technology
Office of Nuclear Regulatory Research
U.S. Nuclear Regulatory Commission
Washington, D.C. 20555

10. PROJECT/TASK/WORK UNIT NO.

11. FIN NO.
B8900

13. TYPE OF REPORT
Technical Report

PERIOD COVERED (Inclusive dates)

15. SUPPLEMENTARY NOTES

14. (Leave blank)

16. ABSTRACT (200 words or less)

Fatigue crack growth rate tests, at a load ratio of 0.2, have been conducted on steels of low, medium and high sulfur contents (0.004%, 0.013% and 0.025%) in PWR water at both low and high flow rates. Crack growth rates show no dependence on flow rate, but are strongly dependent on sulfur content, with a large proportion of environmental assistance for the highest sulfur contents. Tests of low and high sulfur content steels at a load ratio of 0.7 show relatively little environmental assistance in either case. The fractography of these specimens shows the usual brittle appearance for environmentally-assisted fatigue crack growth. In addition, the opposing fracture surfaces match perfectly, indicating that little or no dissolution of the metal matrix has occurred, and there is very little plastic flow associated with the fatigue cracking process. The X-ray photoelectron emission examination of the fracture surface oxides shows that FeS and FeS_2 coexist in the oxide layer, suggesting that the conditions within the crack enclave involved near-neutral pH and cathodic potentials.

17. KEY WORDS AND DOCUMENT ANALYSIS

17a. DESCRIPTORS

Fatigue crack growth
Pressurized water reactor
Hydrogen assistance
Sulfur content
X-ray photoelectron spectroscopy
A 533-B
Load ratio
Flow rate
Fractography

17b. IDENTIFIERS/OPEN-ENDED TERMS

18. AVAILABILITY STATEMENT
Unlimited

19. SECURITY CLASS (This report)
Unclassified

21. NO. OF PAGES
41

20. SECURITY CLASS (This page)
Unclassified

22. PRICE
$

NRC FORM 335 (11-81)

GROWTH RATES IN LWR ENVIRONMENTS